

LOW CYCLE FATIGUE LIFE IMPROVEMENTS REALIZED BY REDUCED  
THERMAL STRAIN DUE TO FLANGE SEPARATION IN BOLTED JOINTS

BY

CHRISTOPHER CARTER

THESIS

Submitted in partial fulfillment of the requirements  
for the degree of Master of Science in Mechanical Engineering  
in the Graduate College of the  
University of Illinois at Urbana-Champaign, 2011

Urbana, Illinois

Adviser

Professor Anthony Jacobi

## **ABSTRACT**

Low cycle fatigue (LCF) life is an essential aspect in aircraft engine component design, particularly concerning structural members. Realistic finite element modeling is critical in obtaining life predictions that accurately represent fielded parts. One of the most challenging designs to model accurately is the bolted joint. Bolted joints are critical in aircraft engines as they connect parts and transfer loads. In complex joints, modeling can be difficult and is often simplified with the use of conservative assumptions. Recent commercial experience on structural hardware exposed to high engine temperatures and pressures has indicated that fielded part life for bolted joint members may be significantly higher than simplified finite element modeling, which includes a number of conservative assumptions, would predict.

Several factors are critical to the quality of a finite element model of a bolted joint. These factors can significantly impact the results for predicted LCF life and can include: proper geometric matching with the actual hardware, appropriate material properties, realistic boundary conditions and suitable heat transfer. This paper will compare simplified 2D modeling of a three flange bolted joint with more accurate analysis taking into account flange separation and leakage. This paper will also attempt to demonstrate that leakage assumptions can impact LCF life predictions. For the joint of concern in this paper, flange leakage is shown to reduce thermal gradients and improve LCF life by approximately 50%. While this paper focuses on only one of the many important facets in bolted joint methodology, effort is made to show the benefit in the inclusion of flange leakage assumptions.

The successfully fielded bolted joint considered in this paper will be examined thoroughly with industry standard methodologies. Finite element models and approaches will be compared between an original model, developed for certification of the hardware, and an updated model which uses the latest in modeling technology. The original model, which used beam elements to simulate the bolt in the joint, did not allow for the full range of flange motion and separation witnessed on fielded hardware. As a result, the applied thermal model did not account for any joint separation or leakage. Temperatures at the joint assumed the flanges were essentially fused together. This resulted in increased thermal gradients on the flange members and lower LCF life then would be expected if the joint were allowed to open. The significant thermal strain resulting from these gradients yields lower LCF life than field experience would suggest. In fact, examination of high life hardware shows no sign of fatigue and this hardware seems capable of service of well beyond the original designed life of the part. This is undoubtedly due to the reasonably conservative nature of the analysis. Again, this paper will seek to understand how the assumptions surrounding joint leakage can impact this analysis. More detailed modeling techniques were recently applied that allow for appropriate separation. Complex thermal models were also modified to rationally account for flange leakage. Although these models yield increased LCF life, flange leakage is only one of the conservative assumptions necessary in bolted joint design.

This paper will also touch on how pairing leakage with material property and convection multiplier assumptions can impact predicted life. Although conservatism is imperative in aircraft component design, this paper will attempt to strip away some of the essential moderation and achieve life predictions that more accurately represent fielded

hardware. Future work will focus on quantifying how these assumptions impact life analysis as engineers strive to create detailed models of bolted joints.

*For my family, Stef, Abby and Sam*

## **ACKNOWLEDGMENTS**

I wish to thank my advisor, Dr. Anthony Jacobi, The University of Illinois, for his encouragement and guidance during my pursuit of an advanced degree.

I also want to thank those who provided technical guidance within GE – Aviation during this study: Scott Ryczek (Structural Design), Curt Stover (Heat Transfer Design), Sachin Rashane (Analysis), and Jan Pirtle (Structural Design).

Finally, I want to acknowledge my family for their support during my studies. The successful pursuit of my advanced degrees would not have been possible without the love and backing they provided.

## TABLE OF CONTENTS

LIST OF FIGURES .....	ix
CHAPTER 1: INTRODUCTION .....	1
1.1 Background Information .....	1
1.2 Field Experience .....	5
1.3 Literature Review.....	7
1.4 Figures.....	10
CHAPTER 2: JOINT DESIGN .....	13
2.1 Design Considerations .....	13
2.2 Joint Description .....	14
2.3 Bolt Design .....	17
2.4 Nut Design .....	18
2.5 Flange Design .....	18
2.6 Material Considerations .....	20
2.7 Joint Preload.....	21
2.8 Joint Behavior Under Load .....	24
2.9 Figures.....	30
CHAPTER 3: ORIGINAL ANALYSIS .....	35
3.1 2D FEA Methodology.....	35
3.2 ANSYS® Elements and Meshing.....	36
3.3 Boundary Conditions and Applied Loads .....	38
3.4 Material Properties.....	42

3.5 Heat Transfer Analysis .....	43
3.6 Structural Analysis and LCF Life Calculations .....	47
3.7 Figures.....	58
CHAPTER 4: IMPROVED MODELING .....	69
4.1 2D FEA Methodology.....	69
4.2 Predicted Flange Separation .....	71
4.3 Revised Heat Transfer Analysis.....	72
4.4 Revised Structural Analysis and LCF Life Calculations .....	79
4.5 Figures.....	80
CHAPTER 5: CONCLUSIONS .....	86
5.1 LCF Life Comparison .....	86
5.2 Ongoing Efforts .....	88
5.3 Figures.....	90
REFERENCES .....	91
AUTHOR’S BIOGRAPHY .....	94



## LIST OF FIGURES

Figure 1: 2D View of Bolted Joint.....	10
Figure 2: Joint Location .....	10
Figure 3: Nozzle Support (Profile, Forward Looking Aft, and Isometric) .....	11
Figure 4: Weibayes Analysis of Fielded Nozzle Supports .....	11
Figure 5: Fielded Flange .....	12
Figure 6: 2D View of Modeled Hardware .....	30
Figure 7: Joint Member Forces (adapted from [4]) .....	30
Figure 8: Stress Distribution in a Typical Bolted Joint (from [4]) .....	31
Figure 9: Typical Stress Distribution in a Nut (from [4]).....	31
Figure 10: Typical Stress Distribution in Joint Flanges (from [4]) .....	32
Figure 11: Effects of Thermal Expansion on Joint Preload.....	32
Figure 12: Example Joint Diagram (from [20]).....	33
Figure 13: Free Body Diagram for the Joint and Nozzle Support .....	34
Figure 14: 2D ANSYS® Model .....	58
Figure 15: Bolted Joint Modeling .....	58
Figure 16: Model Forward Constraints and Loads .....	59
Figure 17: Model Aft Constraints and Loads .....	59
Figure 18: Nozzle Load Detail.....	60
Figure 19: Mission Pressure Profile.....	60
Figure 20: Typical Commercial Engine Mission.....	61
Figure 21: Modeling Bolt Preload .....	61

Figure 22: Hoop Stresses at Takeoff.....	62
Figure 23: Axial Stresses at Takeoff.....	62
Figure 24: Equivalent Stresses at Takeoff .....	63
Figure 25: Temperature Distribution at Takeoff.....	63
Figure 26: Hoop Stress at Thrust Reverse .....	64
Figure 27: Axial Stress at Thrust Reverse .....	64
Figure 28: Equivalent Stress at Thrust Reverse .....	65
Figure 29: Temperature Distribution at Thrust Reverse .....	65
Figure 30: Bolt Hole Nodes Chosen for Life Calculation .....	66
Figure 31: Example S-N Curve.....	66
Figure 32: Example Rainflow Counting Procedure.....	67
Figure 33: Nozzle Support Flange Temperatures vs. Mission Time .....	68
Figure 34: Improved Bolted Joint Modeling .....	80
Figure 35: Rabbet Interference/Gap Definition and Location .....	80
Figure 36: Combustor Case/Nozzle Support Interface Selected Nodes .....	81
Figure 37: Combustor Case/Nozzle Support Interface Gap vs. Mission Time.....	81
Figure 38: Seal/Combustor Case Rabbet Selected Nodes .....	82
Figure 39: Seal/Combustor Case Gap vs. Mission Time.....	82
Figure 40: Combustor Case/Nozzle Support Rabbet Selected Nodes .....	83
Figure 41: Combustor Case/Nozzle Support Rabbet Gap vs. Mission Time .....	83
Figure 42: Original Heat Transfer Model .....	84
Figure 43: Updated Heat Transfer Model .....	84
Figure 44: Flange Temperature Gradients vs. Time Baseline and Improved Model.....	85

Figure 45: Flange Temperature Gradient and Hoop Stress vs. Time .....	85
Figure 46: H Multiplier Impact.....	90

# **CHAPTER 1**

## **INTRODUCTION**

### **1.1 BACKGROUND INFORMATION**

This paper will examine a bolted joint currently in service in one of the world's most successful aircraft engine lines. With a proven track record spanning decades, this family of robust powerplants continues to provide safe, reliable service worldwide. Parts certified for use on these engines were first analyzed in the late 1970s and early 1980s using finite element codes that were just emerging for commercial use. In fact, many of the components in use today are based on previous designs verified primarily with field experience, engine tests, and hand calculations [1]. It has only been in recent years that finite element analysis (FEA) has been useful in understanding the behavior of early, fielded engine components [2]. Today, the finite element analysis method is essential to component design. It allows engineers to adapt approximate solutions to a variety of real world problems. This technique is based on the decomposition of bounded, complex problems into a finite number of elements. Assumed approximating functions are then applied to nodes connecting these elements to arrive at estimated solutions. These solutions are determined through the rendering of partial differential equations into systems of approximating ordinary differential equations, which are solved using standard approaches such as the Runge-Kutta and Euler's method [3].

Early finite element models were limited by computational technology. Models were often simplified due to time and budget constraints as well as modeling capability. Technological progression and improvements in FEA modeling have led to significant

advances in engine performance and optimization. Upgrades in FEA modeling have allowed engineers to remove a great deal of the conservatism necessary in early designs. This has led the way for lighter weight, lower cost engines with improved efficiency. Updated software, like ANSYS<sup>®</sup>, has also been useful in understanding existing designs. Now, more accurately than ever, engineers are able to explore proven components and identify critical and life limiting areas. In this way, engineers can improve on and simplify legacy hardware. Any seasoned engineer would suggest however, that FEA models are only as good as their inputs. Realistic modeling is a function of several key components including part geometry, material properties, boundary and initial conditions, and meshing [4].

The goal of this paper is to examine simplified modeling as compared to more realistic analysis. Specifically, the low cycle fatigue life benefits realized through improved two-dimensional (2D) analysis of bolted joints will be studied. Oftentimes, simplified modeling suffices in non-critical structural component design. In fact, for a number of components a simple shell model with applied stress concentration factors is more than adequate. Although conservatism inherent in design engineering ensures safe component design, realism is traded. In recent years, work has been completed on a 2D ANSYS<sup>®</sup> model of structural hardware in the core of a popular commercial engine. This model was an update to older FEA analysis. In the course of the analysis, several refinements were made: geometry was updated to accurately model the associated hardware, applied heat transfer was correlated to recent tests, and updated modeling techniques were used to represent bolted joints. During this work great effort was made to model the bolted joint as realistically as possible in a 2D axi-symmetric model. For

the bolted joint of concern in this paper, this meant adding in flange leakage assumptions. The hardware surrounding this effort is pictured in Figure 1 and the general location in the engine is shown in Figure 2. The bolted joint in the figure is analyzed here in detail and the flange of the Forward Inner Nozzle Support, visible in Figure 1, is most heavily scrutinized. This flange is analytically known to be the most limiting in the area. The three flanges in the joint of concern are a seal, combustor case/diffuser, and nozzle support. A bolt shield and nut plate are also shown in the figure but are not critical to the joint. These components are in the engine core and exposed to significant loading, temperatures, and pressures. Of the three clamped members in the bolted joint, the plug load and temperature gradient across the nozzle support is known to be the most severe. Primary attention will be given to this component, shown in three views in Figure 3.

The nozzle support is considered a static structural part in that it significantly contributes to the structural integrity of the engine. Although its role in engine architecture is paramount, failure of the nozzle support would not lead to catastrophic failure of the engine. Therefore, it is not considered life-limited hardware and must only meet the more common requirements of the engine's technical document, which defines engine operating conditions, cycle parameters, and expected service life. Generally, structural hardware must be analyzed such that fatigue initiated cracks will be discovered before they propagate to failure. Or, more commonly for this type of hardware, fatigue initiated cracks are not expected during the anticipated useful life of the engine. A typical technical document will require a certain number of cycles for the engine. A cycle, for a commercial application, is a flight profile that would typically include: taxi around an airfield, takeoff, climb, cruise, decent, approach, thrust reverse, and taxi again.

This cycle replicates one typical flight the aircraft might be subjected to and may also include any maneuvers desired by the airframer. Transients may also be defined between the steady-state conditions listed above. Depending on the desired time between steady-state conditions, temperature gradients can be quite severe. It is not uncommon for an acceleration between ground idle, where the aircraft is positioned on the runway, and takeoff to be anywhere from a few seconds to more than half a minute. Naturally the faster the transient, the more severe and potentially damaging it can be to the engine hardware. Thermally induced stresses are most impacted by these transients as hardware heats and cools down at different rates. Larger masses, like bolted joints, tend to heat up and cool down more slowly than thin shells. In the case of a bolted joint, a joint may remain relatively cool while the structures they connect heat up rapidly, resulting in high thermal strain. The rates at which heat is transferred into and out of these masses differs more drastically during rapid transients, driving temperature gradients up. The impact flange leakage has on these thermal gradients is the primary focus of this paper.

With the current 2D ANSYS<sup>®</sup> model, life to crack initiation is X cycles. For the basis of this paper, fatigue life, joint stresses, and temperatures will be normalized or omitted, as design specifications and cycle parameters are proprietary information. Also, a cycle as defined above will include one major LCF cycle. This LCF cycle was identified for this hardware through a rain flow analysis of mission stresses at the joint. Although several minor cycles also exist, particular attention is given to the major cycle. More fidelity is generally required around the major LCF cycle and particular attention is given to associated time points. If the current predicted baseline life for the joint is X cycles, field experience suggests life exceeding 4X cycles.

## 1.2 FIELD EXPERIENCE

Although current analysis suggests the nozzle support flange will crack at X cycles, no evidence of fatigue is witnessed on fielded engines. In fact, engines used for endurance testing and those examined during shop visits show no signs of distress at the flanges of this joint whatsoever. Instead, parts examined suggest continued life exceeding the original design intent. With the high production volume over the past several years, cracking or signs of fatigue could be expected on some of the most high time parts.

Statistical analysis using Weibayes methods suggests that fatigue life in the joint is 3X. Data collected on fielded engines in 2009 revealed average life of 2X with some engines exceeding 4X. Again, for the basis of this paper, X is considered the predicted fatigue life of this joint based on current modeling. This population, over 4,000 engines, is sufficient that cracking would be expected if ANSYS<sup>®</sup> modeling were completely accurate. Although the model and analysis were constructed with conservative assumptions concerning material condition and factors of safety, cracking should be present on at least some of the fielded parts. From a statistical standpoint however, a Weibayes analysis is sufficient to set the bar for expected life.

Weibayes is a method for constructing a Weibull distribution based on knowing or assuming a Weibull slope parameter. It can be used when there are few or even no failures. Used extensively in aerospace applications, Weibull analyses are useful in predicting life to failure when little data exists concerning failure and time or funds are not available for testing. In Weibayes analysis, the slope or shape parameter,  $\beta$ , is assumed from historical data, prior experience, or engineering knowledge of the physics



of failure. In this case  $\beta$  is assumed to be one although experimentation with other slopes indicating wear out ( $\beta > 1$ ) shows similar results. The following equation applies for characteristic life [5]:

$$\eta = \frac{\left[ \sum_{i=1}^n t_i^\beta \right]^{1/\beta}}{r} \quad (1)$$

Where,

$t_i$  = time or cycles on unit  $i$

$r$  = number of failed units (Assume  $r=1$  for zero failures)

$\eta$  = maximum likelihood estimate of characteristic life

$n$  = total number of units

With  $\beta$  assumed and  $\eta$  calculated from the equation above, a Weibull distribution is derived. Since no failures have occurred,  $r$  is assumed to be one, i.e. the first failure is imminent. The equation then gives a conservative 63% lower confidence bound on the true value of  $\eta$ . For this analysis WinSMITH<sup>TM</sup> was used. WinSMITH<sup>TM</sup> is a widely available Windows based probability-plotting program. From the resulting probability plot shown in Figure 4 it is evident that expected life is much higher than the X cycles predicted by the FEM [5].

As component life information is proprietary, axis information for the probabilistic plot has been removed. Even if we assume the first failure is imminent, a Weibayes analysis suggests higher life than 2D modeling. As we will see, there are several areas surrounding the joint modeling and assumptions where conservatism may be a factor.

Of the critical elements in component modeling, this paper will examine flange temperature distribution on the nozzle support as impacted by flange separation and joint leakage. As noted earlier, the current model does not account for flange separation caused by joint prying. This separation is believed to cause leakage, which greatly reduces the temperature variation radially across the flange of the nozzle support and lessens thermal strain. This effect is believed to be most significant during mission transients. Again, no indication of flange distress is noted in the field. Fielded nozzle supports do however show noticeable changes in oxidation patterns on the forward flange. The flange in Figure 5 shows evidence of changes in surface contact between the nozzle support and combustor case as indicated by discolored areas.

The inside diameter of the flange, where the nozzle support remains in contact with mating hardware, appears darker. An amber color can be easily seen from the bolt hole to the inner diameter. The outside diameter of the flange is lighter, suggesting exposure to elevated temperatures. This bluing is typical of hardware exposed to temperatures at the combustor, which lies just above the joint of concern. Further definition of this joint, its flanges, temperature distribution and loading will be detailed in later chapters.

### 1.3 LITERATURE REVIEW

Little information could be found relating to flange separation and leakage in non-gasket joints. While a great deal of emphasis has been placed on bolted joints in highly loaded pressure-vessel-type applications, more scrutiny is usually given to the bolt than the flanges themselves. In fact, several published articles go into significant detail

concerning the factors affecting preload, thermal impacts on joint behavior, finite element analysis modeling and flange stiffness. More often than not however, these articles deal with gasketed joints and do not to quantify leakage impacts or study flange distress. Bolt fatigue, for example, is studied by Hagiwara and Yoshimoto [6] for cylindrical and T-flange joints. Bolts in cylindrical joints, they surmise, are only truly subject to fatigue when contact surfaces fully separate. No analysis is presented for the flange members. Extensive information is available to document modeling impacts on predicted bolted joint behavior. Of late, this analysis is often complex and shown to be best represented with 3D modeling [7-8]. Due to the complexity of bolted joints in aerospace applications, this paper will focus on 2D modeling which has been shown to be viable by Spence *et al.* [9] and Nash *et al.* [10]. An article by Fukuoka [11] even examines bolted joint preload variations due to small gaps in mating components through 2D axisymmetric modeling. Additional information is discussed in subsequent chapters [12-14].

Thermal effects on bolted joints are analyzed in detail by Bouzid *et al.* [15-16, 17] where stiffness, creep and thermal distortion are studied to assess their impacts on bolt and gasket load. Creep and stiffness effects are well documented and applicable here in a discussion of joint design and preload considerations. Sawa *et al.* [18] also examine gasket stress relating to differences in bolted joint temperature. In the available literature, temperature impacts due to leakage have been all but ignored. In fact, Fukuoka [11] uses an FEA model to predict bolt, nut and flange material coefficient of thermal expansion changes due to leakage and relates these findings to bolt stress while Hyde *et al.* [19] quantify predicted joint gaps and resulting leakage. These authors do not attempt to

determine flange impact. These texts, as well as accepted design references, tend to focus on leakage elimination or minimization. Perhaps the best known authority on bolted joint design is John H. Bickford. His most notable works, An Introduction to the Design and Behavior of Bolted Joints, and Handbook of Bolts and Bolted Joints deal considerably with joint design of the type represented by the nozzle support flange. Again though, most of the concentration in these texts is placed on the bolt. According to his texts, for tensile joints, the bolts should clamp the joint members together with enough force to prevent them from separating or leaking [4]. Concerning joint fatigue, he suggests that failure only occurs under tensile loads at the bolts. Any indication of temperature gradient impact due to joint leakage is omitted and flange failure is generally not discussed.

Several journals and texts reference the prying action in eccentric joints. This information is used to examine the joint of concern in this paper. The design of this joint was based primarily on engineering experience, component and engine tests, and controlled design practices. Some of the analysis performed for the joint was done using best practices and proprietary information belonging to the General Electric Company. Therefore, great effort is made in this paper to exclude this type of information. Instead, commercially and academically available references are cited and joint detail and analysis methods are noted only where necessary. In fact, the key aspects of this bolted joint design may be wholly examined with openly available journals and texts for the purposes of this paper. Where necessary, information relating to specific, controlled design assumptions, constraints, inputs and methodologies is omitted.

## 1.4 FIGURES

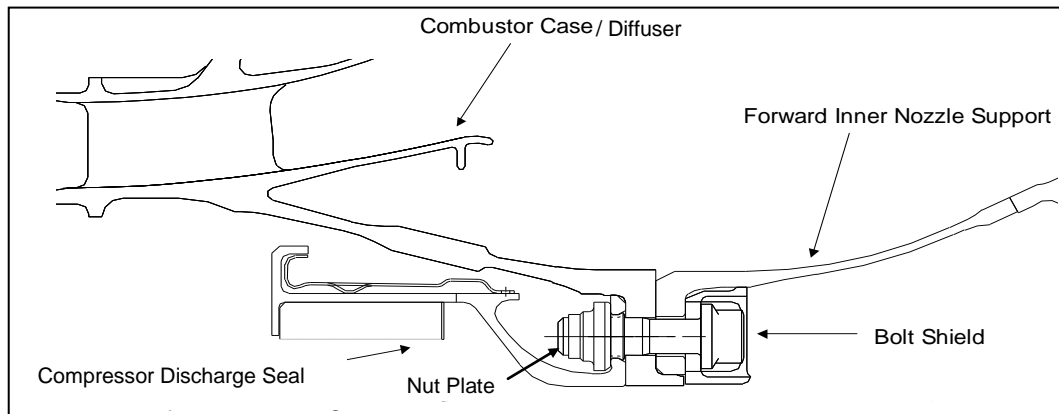


Figure 1: 2D View of Bolted Joint

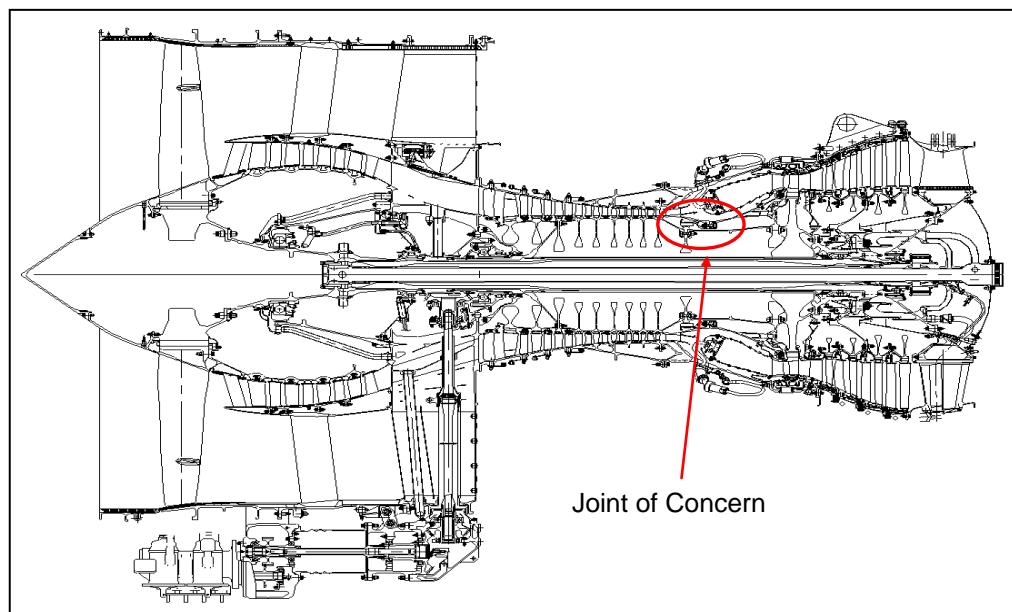


Figure 2: Joint Location

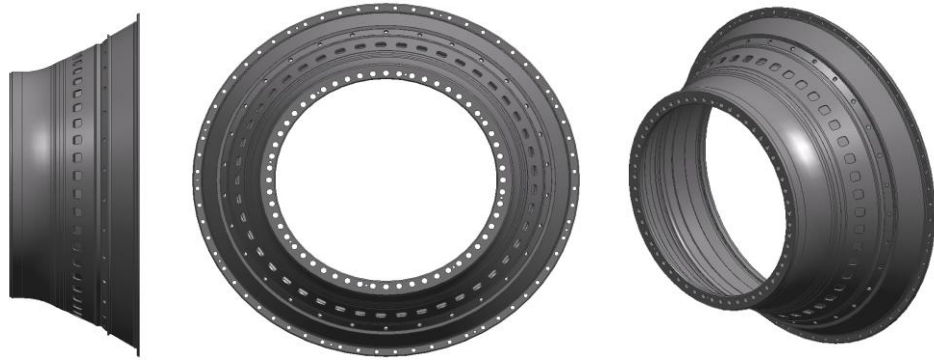


Figure 3: Nozzle Support (Profile, Forward Looking Aft, and Isometric)

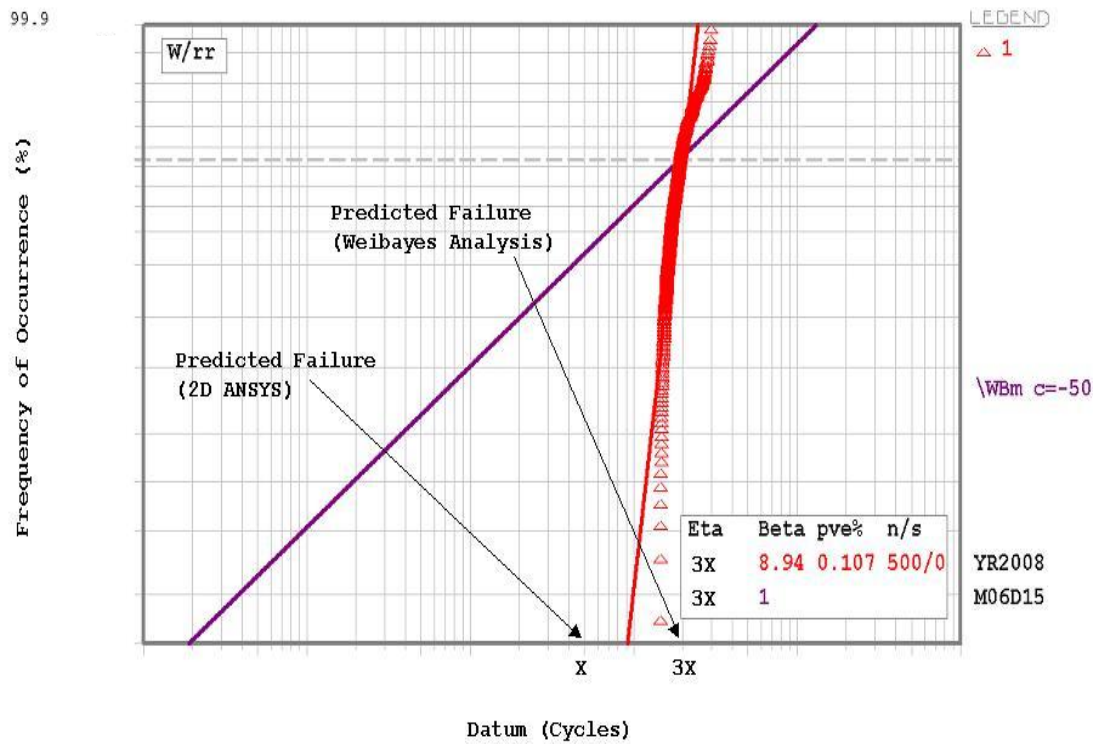


Figure 4: Weibayes Analysis of Fielded Nozzle Supports



Figure 5: Fielded Flange

## **CHAPTER 2**

### **JOINT DESIGN**

#### **2.1 DESIGN CONSIDERATIONS**

Although the original design of this hardware was done decades ago and updates based on engine test and improvements in analysis capability have been made, effort is made in this paper to explain the joint using common industry terms and analysis methods. Barring use of any specific design practices and proprietary information, Bickford's texts are used to detail the joint sufficiently for basis of this paper. Figure 6 shows components critical to the understanding of this joint and the boundary conditions necessary for proper design and analysis.

In this model, from the front of the engine aft, we note a portion of the combustor case, the compressor discharge seal, the forward nozzle support, the aft nozzle support, and an outer stationary seal. More detail of this hardware will be provided in the following chapters. Design functions will not be discussed as they relate to proprietary information. Again, the bolted joint in black is the area of concern for this analysis. These parts are structural and make up the core of the engine, supporting both the combustion chamber and high pressure turbine nozzle. For the 2D ANSYS® model discussed in Chapter 3, the above hardware is considered and LCF life on the blue nozzle support is determined. Housed in the engine's core, these components are exposed to elevated temperatures, pressures, and carry the loads imparted by the high pressure turbine nozzle. This load is reacted forward, through the forward flange of the forward nozzle support to the bearing.



When setting out to design a bolted joint such as this, it is the design engineer's goal to select bolt and joint geometries and materials that will guarantee enough clamping force to prevent bolt self-loosening, joint slip, separation, leakage, and fatigue [4]. This is a very difficult undertaking however, and great care is necessary concerning joint design and sizing. More often than not, each bolted joint the designer analyzes is unique. Therefore, adherence to edicts or proscriptions laid out in engineering handbooks must be supplemented with sound engineering judgment, prior experience, and the use of complex models where necessary. Indeed, bolted joints are often the weak links in structural loads paths. Proper conservatism is a must for reliable designs. Keeping in mind the design goals above, this paper will focus on flange fatigue and leakage due to prying of the joint. The original design of the bolted joint in question was done more than 20 years ago. Although the preliminary joint sizing, initial design, detailed analysis, and testing have been completed, this paper will highlight considerations applicable to the understanding of the design.

## 2.2 JOINT DESCRIPTION

The joint in question is a tensile joint and the bolt is designed such that it will exert as much force on the joint members as they can stand. The bolt is the only mechanism for creating and maintaining the clamping force between members. The magnitude and stability of that clamping force governs the behavior and life of the joint. The clamping force is initially created at assembly when the bolts are tightened. This creates tension in the bolt as preload is set. The flanges, or joint members, in contrast are compressed as indicated in Figure 7 adapted from Bickford [4].

Essentially, the joint members act as stiff springs, storing potential energy exerted by the bolt. The challenge is maintaining that potential energy throughout the duration of the joint's serviceable life as several factors attempt to lessen it. Evaluation of a bolted joint design, once applied loads are known, starts with an understanding of these springs. A key component for consideration is the relationship below. Known as the axial flexibility ratio for the joint, we note that clamped and clamping members are represented by spring constants.

$$\text{Axial Flexibility Ratio} = R_a = \frac{K_{CLAMPING}}{K_{CLAMPED}} \quad (2)$$

Here  $K_{CLAMPED}$  represents the series-spring combination of all the clamped elements in the joint (flanges) and  $K_{CLAMPING}$  is the series-spring combination of the clamping elements in the joint (bolt). Analysis of the bolt is a straightforward calculation of the spring rates of the various cylinders in series that make up the bolt (shank, threads, head, etc.). It is desirable to keep the flexibility ratio less than 0.5 throughout the engine cycle, meaning that the clamping member stiffness is no more than 50% of the clamped members. This can help minimize cyclic loads on the bolt and improve fatigue life [20].

For the clamped spring elements, each flange must be considered individually. The process of determining the term  $K_{CLAMPED}$  consists of determining an equivalent cylinder diameter and length for each member in the joint. The individual spring constants are functions of the cylindrical areas under the head of the bolt and nut ( $A_S$ ), lengths ( $L_J$ ), elastic moduli ( $E_J$ ) of each member ( $J$  denoting member number) and is

determined by:

$$K_J = (E_J \times A_S)/L_J \quad (3)$$

For a conventional flange, the compressed area spreads out in a barrel shape into the surrounding material so that the equivalent compressed area becomes difficult to estimate. The above relation, however, suffices for design considerations. Once the spring constants of the various cylinders involved are determined, the flange spring rate,  $K_{CLAMPED}$ , can be calculated by a combination of springs in series.

$$\frac{1}{K_{CLAMPED}} = \sum_{n=1}^{NF} \frac{1}{K_n} \quad (4)$$

These calculations can become time consuming for multiple flanges or when evaluation is necessary at a variety of temperatures. For our use, only two temperatures are considered, temperatures at assembly and takeoff. These time points represent the minimum and maximum temperatures to which the joint is subjected. This is just one consideration when sizing a bolted joint. There are several other factors that impact joint behavior. Effects on the joint from thermal and mechanical loading are evident. Changes in modulus, joint preload, and deflections based on external loading can all impact these calculations. If these environmental changes are significant, care should be taken in obtaining and maintaining high preload. Many of these factors will be discussed in later sections of this paper but, for initial joint sizing, choice of the appropriate axial flexibility ratio is fundamental.

## 2.3 BOLT DESIGN

The bolt in this joint is an MP159, double-hex head, spline-drive, reduced shank fastener that is 3/8" in diameter. Material design curves based on industry and company tests suggest the ultimate tensile strength of the material is more than sufficient to ensure joint integrity, even at elevated temperature. This type of bolt, Figure 8, is typical in aircraft component design. Assembled with 550 lb-in of torque, graphite-petroleum grease is used to lubricate the threads. Again, this bolt is common to aircraft engine hardware and well within the design experience established over several years with successful engines. Although the bolt is industry standard, its application here ensures that stresses remain well below the yield strength of the material at temperature under the maximum separating tensile load. The engine mission typically defines the maximum separating load. Engine imbalance, defined flight maneuver loading, and mechanical and thermal loads applied to the hardware couple with established factors of safety to define this load. The maximum separating load is then compared to the average clamp in the joint that has been reduced due to torque variation and adjusted for elastic and inelastic effects attributed to in-service use.

This joint is a tensile joint and the members are subject to large plug loads. We expect a stress distribution as depicted in Figure 9. While the simplified distribution assumes a pure tensile load in the bolt shank, the figure is adequate in understanding how joint members interact. The shank is held in tension by compressive forces in the nut, flanges, and bolt head. Again, this model ignores local stress concentrations due to threads and neglects stresses imparted by torsion, bending, and shear. We will see however, that 2D modeling shows similar stress gradients in the flanges [4].

## 2.4 NUT DESIGN

The nut in this joint is a sub-assembly of a nut plate. Only the nut will be considered here however, as the 2D model is only a representation. The nut plate does not significantly impact the joint in terms of clamp or stiffness and its inclusion in the axial flexibility ratio calculation would be insignificant. The nut is a silver plated self-locking clinch nut made of Waspaloy. The design is an aerospace standard, thin-walled design, which distributes load among the maximum number of threads, providing optimum strength and life for the bolt. Use of Waspaloy also helps ensure the nut has greater overall strength than the bolt. Silver-plating is applied to the threads for added anti-seize protection during repeated assembly and disassembly. We may also note that the nut is low profile. Decades of experience indicate that increased nut height does not reduce peak stresses as only the first few threads carry significant load. For that reason, low-profile nuts are generally used to aide in engine clearances and reduce engine weight. Lines of constant stress are shown in Figure 10 for a typical nut in tension. Note that this figure comes from Bickford's texts and shows lines of constant stress for a bolted joint loaded in tension with 100 ksi [4]. The 100 ksi is evident through the net section of the bolt shank. It quickly decreases through the nut with significant bending at the mating faces. A similar distribution may be expected in the head of the bolt.

## 2.5 FLANGE DESIGN

The flanges of this joint are designed such that the bolts are closely spaced. This will help minimize the risk of leakage and ensure proper clamp. Excessive leakage in this area is costly as air is taken from the combustion chamber. Air removed from the

combustion chamber is not converted into thrust and represents a negative impact to engine performance and efficiency. Essentially, work done by the compressor is lost and not turned into thrust, used to control flows, or cool high temperature components. The flange is also designed with a rabbet at the combustion case to nozzle support interface. This rabbet helps maintain concentricity throughout the engine mission. Of the three members in the joint, the forward seal is made of a low thermal expansion Inconel alloy while the combustor case, nozzle support and bolt shield are all made of industry standard Inconel 718. The flange also contains several jackscrew holes for use during disassembly. These holes are not considered here since they do not impact joint clamp and are not included in the 2D model. Stresses at these holes were considered in the original design of the joint and in the hoop direction, are shadowed by the larger bolt holes. Hoop stress, due to thermal strain, is the more significant stress at the flange.

Flange stresses are detailed in Figure 11 from Bickford. Just as before, this is a simplified model and represents lines of constant stress in a tensile joint subjected to a 100 ksi load. Its use here is adequate however, in understanding how this joint behaves. Flange compression in the clamped members is evident in the bowed lines of constant stress. Contact pressures between the nut and bolt head, and the joint members cannot be expected to remain uniform. Instead, unaligned planes and variations in surface condition generally impart more irregularity than is represented here. Also, the nut and bolt heads could be expected to embed slightly, allowing stress relaxation. We will see later however, that the 2D model of this area shows a similar pattern for lines of constant stress [4].

## 2.6 MATERIAL CONSIDERATIONS

Materials for this joint, as noted in the preceding sections, were chosen for their physical and chemical properties as well as their known widespread use in the aviation industry. Like the preload established at assembly, material properties play an important role in maintaining the appropriate joint clamp in service. For the bolts, the tensile strength of the material is most critical. For any given diameter and thread configuration, stronger materials will yield stronger bolts. Thermal expansion is also an important characteristic in material selection. Temperature changes will invariably alter the length of the bolts and the thicknesses of the joint members, which can impact joint clamp. Material properties of the joint members of concern have been selected such that their thermal coefficients of linear expansion are low and well matched over the given operating conditions.

The members in this bolted joint are strain controlled. As such, stress relaxation due to the slow reduction in load under constant deflection can be expected. The initial tension in the bolt will gradually be reduced during engine operation due to exposure to high temperatures for prolonged periods of time. The materials of the bolted joint are classified as exotic aerospace bolting materials useful at high temperatures and are designed such that they still retain enough strength and energy storage capacity to be useful during engine operation. Despite this, Bickford notes that the elements that lead to relaxation are many and hard to predict. Relaxation can never be fully guarded against, especially when designs are weighed against part cost and producibility [4].

## 2.7 JOINT PRELOAD

The preload in this bolted joint was established with decades of torque-tension test data on the members in question. These tests included various bolt, nut, assembly lubricant, and joint designs as well as bolt on block tests during which torque was applied to joint configurations and tension was measured. Over time, these measures of tension compared to torque applied yielded sound relationships available for statistical use in continued joint design. Assembly lubricants are used to allow more repeatable torque application, but are not useful after engine operation. For that reason, nut anti-seize coatings are used. Torque is achieved with the use of standard industry tools and practices. This torque provides a certain preload with reliability determined by Six Sigma standards. Preload or initial clamp, as Bickford makes the distinction, must be high enough to compensate for embedment relaxation, elastic interactions, creep, external tensile loads, hole interference, and thermal expansion [21]. Again, decades of engine tests suggest the preload applied in this joint is adequate. The importance of correct preload cannot be overstated. Insufficient preload can cause corrosion, fatigue failure, mechanical failure, self-loosening of the fastener, and leakage [4]. When determining preload, the elastic effects on the joint members in operation at elevated temperatures must also be considered. Forces acting to reduce preload can be considerable even when all materials are the same. This is true primarily because the flanges, bolt, and nut are not usually at the same temperature. This results in a loss of bolt load and simple thermal growth relations can be used to calculate impacts. It is also important to note that the elastic moduli of the members also change with temperature. An example of thermal expansion effects is shown in Figure 12. Note that the fastener and flanges are different



materials and expand at different rates. In the figure the flanges and fastener are assumed to be at a uniform temperature. As this temperature increases, the joint members expand at different rates. This difference in expansion, or delta, is analogous to a loss in clamp. This is just one example of how temperature can impact joint clamp.

In addition to the effects noted above, there are several inelastic effects that can impact preload during service. These effects are usually time and temperature dependant. Bolting materials have a threshold temperature below which creep and relaxation mechanisms are insignificant and need not be considered. Although the members in this joint are not pushed beyond their threshold, elevated temperatures over long periods of time can be harmful. Also, these joints are repeatedly disassembled and reassembled during the engine's regular shop visits for maintenance and inspection. Retorque during these shop visits can also impact preload. For the basis of this paper however, only elastic effects are considered.

Considering the elastic behavior of the joint, some attention will be given to the joint diagram to show the behavior of the flange under load graphically. An example taken from a technical paper by GE - Aviation Chief Engineer Robert Czachor is shown in Figure 13 [20]. It is imperative that engineers designing bolted joints understand that load applied to a joint is absorbed into both the clamped members and the bolt. Czachor notes that load is split as defined by the joint spring constants and axial flexibility ratio. This load results in increased bolt tension and flange compression relief.

As Figure 13 illustrates and Czachor's article notes, bolt load is initially reduced due to thermal effects. The joint members expand and elastic moduli decrease. Although bolt load does increase under engine operating conditions, it is mainly joint compression

relief that absorbs load. As the load increases further however, there is a noted change in slope of the bolt load versus applied load curve. This indicates the point of separation where clamp at the bolt centerline is lost, noted by the C on the chart. This is also the point at which the joint is considered to have failed. Beyond this point, increased load plastically deforms the bolt, compression at the flange toe is completely relieved, and bolt fracture is imminent [20].

In the harsh environment of the engine's core, hundreds of variables exist that work against clamp. The average preload in this flange is several thousand pounds. Field experience and hardware testing suggest this is more than enough preload to ensure flange leakage is kept to a minimum and separation is guarded against throughout the engine's mission. Bickford however, would argue that every joint, especially non-gasketed joints, should be expected to leak. In this case of this joint, leakage estimates have been identified and deemed acceptable by engine performance, safety, and secondary flows experts. In fact, leakage was assumed to be so small that it was not originally accounted for in the stress model. Further, any leakage that does occur has been accepted through engine test and efficiency ratings. For that reason leakage was ignored and not examined for any beneficial impact it might have in terms of thermal gradients through the flange. Although the impacts to engine performance and safety may be small, nearly every tensile bolted joint will experience an increase in tensile load that will decrease the clamping force in the joint. It is this loss of clamp that this paper seeks to understand in terms of LCF life. The many and varied causes of clamp loss and the difficulty one has in estimating it lead to Bickford's "First Law of Bolting: Most bolted joints in this world are providing less clamping force than we think" [4].

Among the factors that can impact joint clamp, stress relaxation is a major concern, but one engineering best practices protect against. Studies have shown that immediately upon completion of bolt torque in steel members there is a two to 11% drop in load. These studies suggest that the average load loss is around five percent and is expected to be the result of elastic recovery of the joint when the wrench is removed. As these studies have shown, predicting load loss is no easy task. Time, temperature, and high stresses are also fundamental causes of relaxation and things design engineers should consider carefully. While time and temperature may be well below creep limits, relaxation can occur as the material ages. Indeed, it would be a significant undertaking to attempt to quantify load loss for any particular design and include all possible sources. Designed-in factors of safety help provide a measure of assurance against joint relaxation [22].

## 2.8 JOINT BEHAVIOR UNDER LOAD

The joint of concern for this paper is primarily subjected to a separating load applied parallel to the axis of the bolt. Transverse loading, although a key design point, is therefore not considered here. The loading is also assumed to be axisymmetric in that it is constant around the joint circumference and no significant geometric peaking factors are present. The most significant load acting on this joint is the plug load imparted by the internal engine pressures acting across the shell of the nozzle support. This plug load, applied eccentrically, attempts to separate the flanges at the joint. The bolted joint was designed such that the bolts would provide a certain minimum clamping force under the maximum in-service loads with a specified margin included. These loads are defined in

more detail in Chapter 3 but their resultant impacts at the joint of concern are noted here. Before addressing the in-service design considerations, this paper will briefly examine the free body diagram of a typical bolted joint loaded in tension. The diagram shown in Figure 14 shows the nozzle support flange of the joint with applied forces. In the figure we only focus on the nozzle support since prior, similar engine designs have shown this to be the most loaded flange in the joint. Although the figure is simplified in its treatment of the local geometry of the joint, this free body analysis is the preliminary methodology used to design the joint. In fact, for complete analysis, interface loads are typically taken from a 2D model of the joint and reacted out to the shell. In this way, loads are conservatively applied to a beam approximation taking out any bending that may exist in the actual part.

With the above basics, we are able evaluate the joint. For this analysis, the joint is assumed to be a non-separated joint, meaning that we assume the applied loads are low enough that clamp at the bolt centerline is not lost. A separated joint, in contrast is a joint that has lost clamp at the bolt centerline. This non-separated joint assumption is valid since fielded hardware does not indicate separation at the bolt hole centerline. For fielded engines separation only occurs at the flange outer diameter and does not extend as far inward as the bolt hole. Analysis of a separated joint, in which contact is lost at the bolt centerline, is typically done assuming severe ultimate loading conditions. This analysis was conducted on the bolted joint prior to engine certification and took into account extreme flight maneuver loads as well as fan blade out loads but is not within the scope of this paper. Instead, we will limit our study of the bolted joint to observed behavior.

The following calculations are useful in determining reliability of the joint. In fact, bolt tensile load and bending moment in operation, bolt stress range, flange moment, and separation margin are just a few of the several factors that are carefully considered during bolted joint design. Referring back to our free body diagram for the single nozzle support flange, the following methodology to determine separation margin may be applied for the common case of a positive tensile separating load and flange toe reaction. Again, separation is considered loss of clamp at the bolt centerline. Separation margin then, is a measure of closeness a bolted joint is to a theoretical, calculated load at which the joint separates. As discussed previously, sufficient separation margin is a must for successful bolted joint design. In addition to flange leakage, separation can lead to bolt fatigue and other detrimental events. The free body diagram includes all applied and reacted loads, which must balance for the nozzle support flange. Dimensions are listed generally from the bolt centerline and flange forward face. Nomenclature is taken from available literature [20]. In his article, Czachor uses a similar free body diagram and we may note that the toe reaction distance,  $b$ , represents the distance from the bolt centerline to the centroid of the distributed reaction force. Analysis of the free body diagram reveals that this dimension is critical to the applied bolt load. Although the reaction force may be spread along the flange face, the centroid is where we consider application for the following calculations. The dimension  $b$  should be consistent with the hardware geometry and should be biased towards the smallest of all possible values. A small  $b$  will increase the bolt load conservatively per the following calculations. As a minimum we note that  $b$  must be greater than half the diameter of the hole, meaning that the reaction force cannot act within the bolt circle.

$$b \geq D_h/2 \quad (5)$$

Analysis of the free body diagram leads to the following equation for applied bolt load as a function of flange geometry, location of applied loading, and the axial and radial forces and the moment acting at the arm cut boundary.

$$B_{Applied} = \frac{1}{b} \left\{ P(l+b) + M_s + L_r \left( L_x + \frac{t}{2} \right) \right\} \quad (6)$$

The above equation is taken from Czachor's article on bolted joints. Given the applied axial load,  $P$ , and applied bolt load,  $B_{Applied}$ , the value of  $R$ , the toe reaction, can be calculated by axial equilibrium.

$$R = B_{Applied} - P \quad (7)$$

With  $B_{Applied}$ , we must now find the theoretical load at which the joint will separate. Using relative axial flexibility, the remaining term becomes the following.

$$B = B_{or} + B_{Applied} \times \frac{R_a}{(R_a + 1)} \quad (8)$$

Note here that  $B_{or}$  is defined as the bolt preload in operation. This takes into account the initial preload and losses that occur due to Poisson's contraction, and joint growth and modulus changes due to increased operating temperatures. As noted earlier, these only a few of the many factors that impact preload during operation. For this

analysis however, these factors are believed to be the most significant driver of clamp loss. Although no effort is made to include other factors, separation margin may be calculated by the equation,

$$\text{Separation Margin} = \left\{ \frac{B_{or} (R_a + 1)}{B_{Applied}} - 1 \right\} (100) \quad (9)$$

It is important to note that separation margin, as defined here, only guards against loss of clamp at the bolt centerline. Some small amount of separation can certainly be expected in any bolted joint under load. It is also important to reiterate, that separation margin is only one of the several factors used to determine soundness of a joint design. Other checks are also important. Bolt stresses must be fully examined. The preload necessary to guard against joint separation cannot be so great that assembly torque could cause bolt rupture. During the mission it is important that the bolt remain horizontal and that loading does not cause bolt bending. Bolts in tensile joints should act in tension and are not meant to take significant bending loads. Excessive bending can lead to low cycle fatigue, another concern in joint design. Preload should be managed, keeping alternating stresses low and well within the LCF range for the bolt material. In addition to the bolt, flange stresses and bending should be monitored. As in the predicted case for our joint, high alternating stresses in the flange can cause joint failure. Likewise, moments exceeding the natural overturning moment for the flange can be significantly detrimental. Rabbets, the nut, and bolt head should also be checked to ensure crush is not an issue. Finally, transverse loads need special attention to ensure flange capabilities are not surpassed and tear-out is not a concern. Again, this is not an exhaustive list of joint

design considerations. This information is presented to give a sense of the many and varied aspects of the initial joint design. During engine certification detailed calculations were performed showing satisfactory margin to these and several other design parameters and the joint was certified as reliable.

In addition to Bickford's texts, the joint may be analyzed assuming it behaves like simply connected beams. Using a true beam theory methodology we may analyze the joint against several of the design criteria above. In fact, beam theory can be used to determine the theoretical point at which the bolt will fail and predict detailed information regarding applied loading, reaction forces, bolt and flange moments, and separation. Simple shell models may be created to use beam-approximating techniques. All this is typically done early on the design phase when geometry is still preliminary. With these calculations and methods engineers can quickly gage feasibility of a design without beginning the full, complex analysis that can take significantly more time. Once these initial design criteria are met, more detailed ANSYS<sup>®</sup> modeling is generally conducted. In the case of the nozzle support flange, recent modeling revealed higher stresses and lower LCF life than originally thought. In his texts, Bickford notes that LCF capability need only be evaluated at the bolt threads. Fatigue in tensile joints, he asserts, is witnessed only in the bolts. Recently updated 2D modeling for our joint suggests otherwise. This paper will examine differences bolted joint modeling methods and how leakage assumptions can impact the joint design.



## 2.9 FIGURES

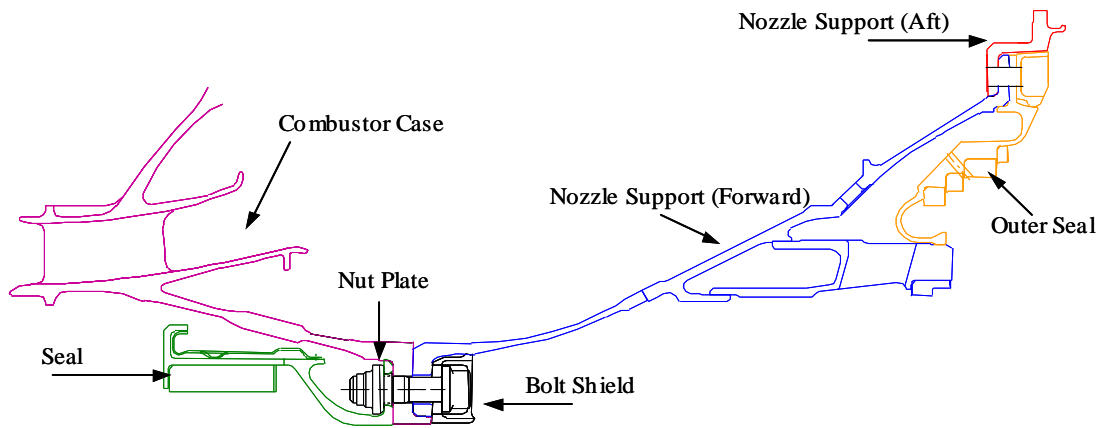


Figure 6: 2D View of Modeled Hardware

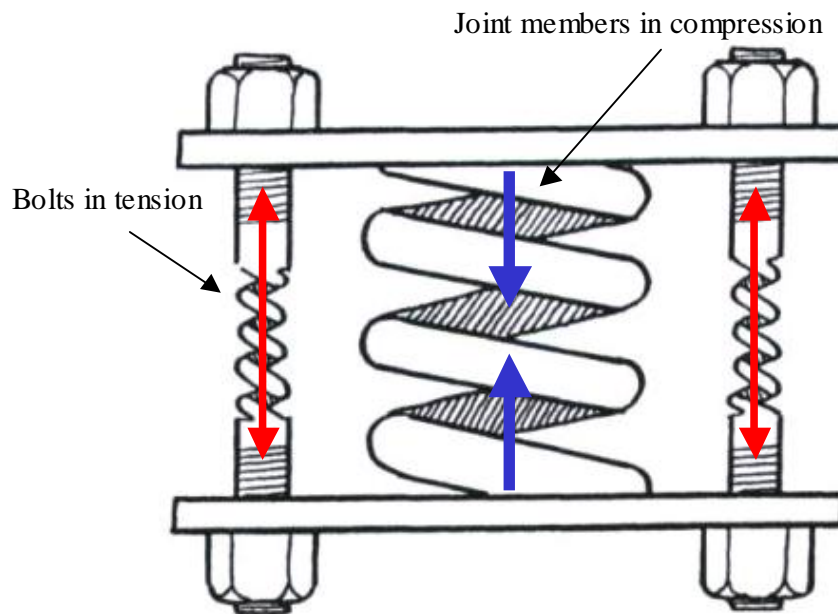


Figure 7: Joint Member Forces (adapted from [4])

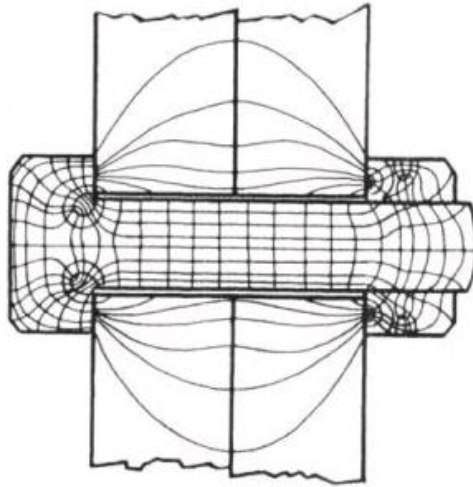


Figure 8: Stress Distribution in a Typical Bolted Joint (from [4])

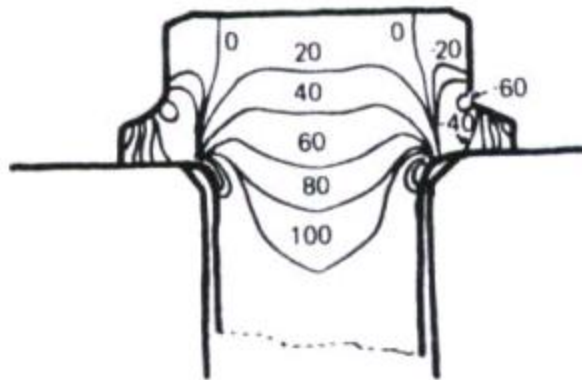


Figure 9: Typical Stress Distribution in a Nut (from [4])

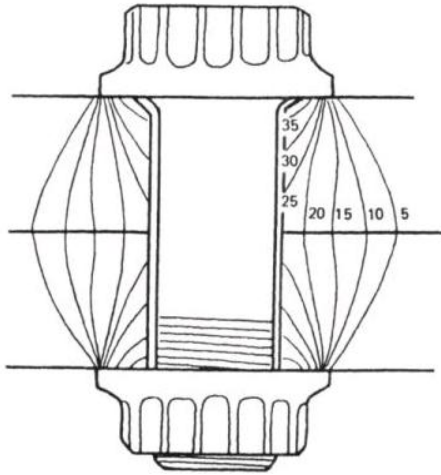


Figure 10: Typical Stress Distribution in Joint Flanges (from [4])

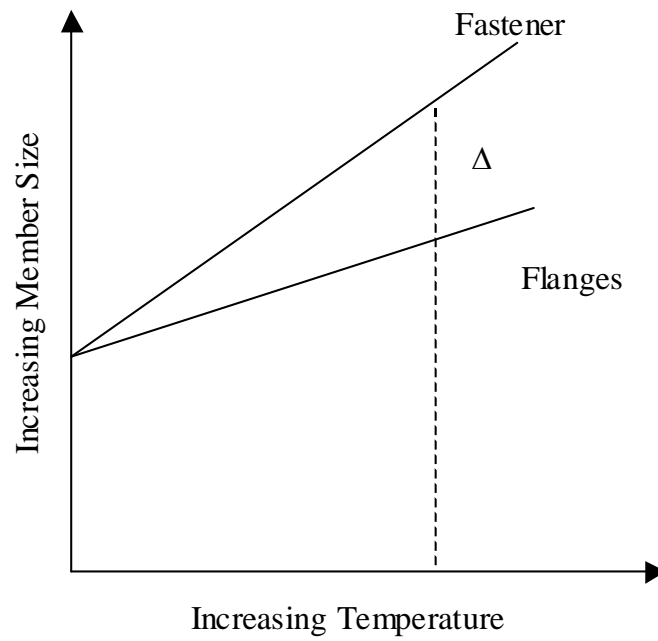


Figure 11: Effects of Thermal Expansion on Joint Preload

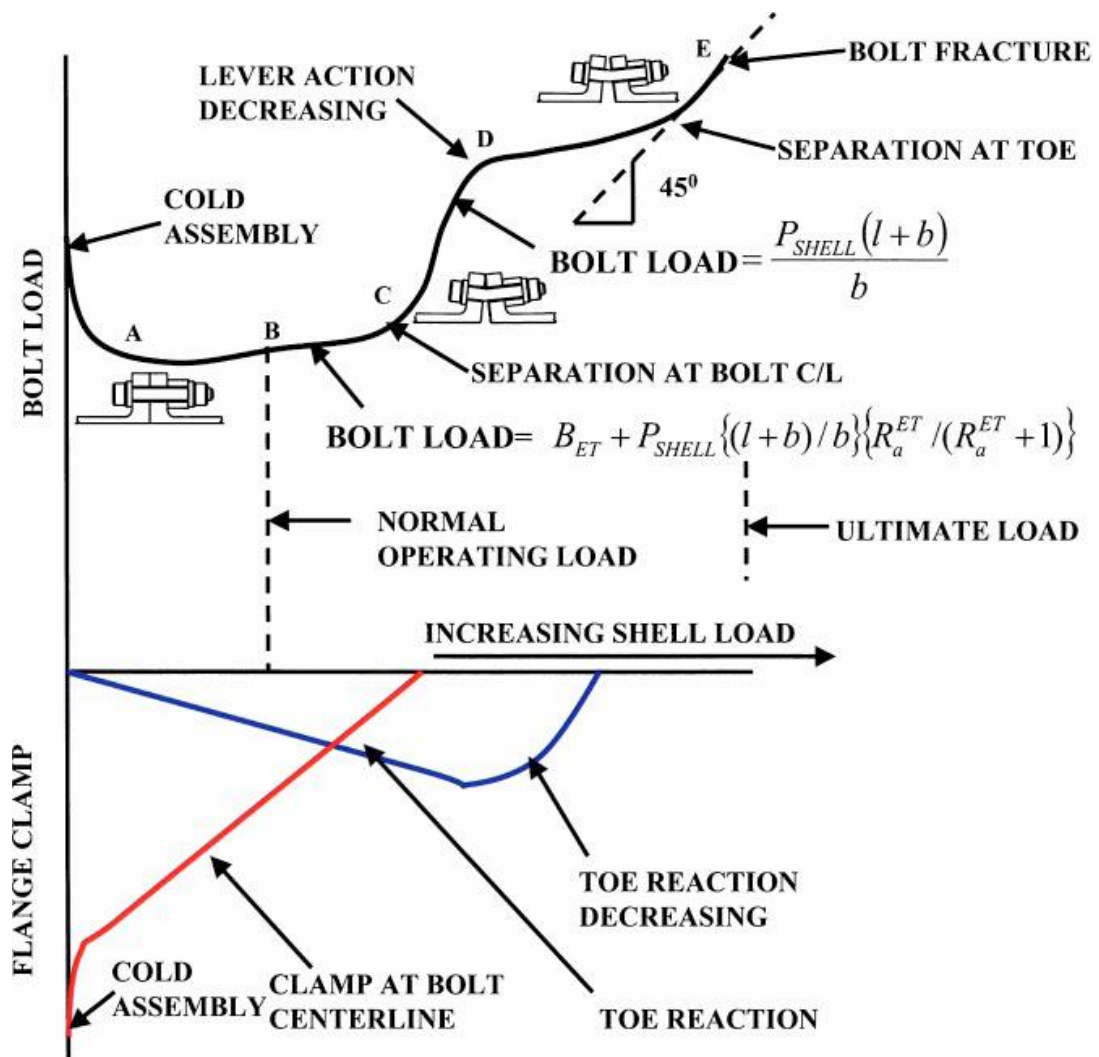
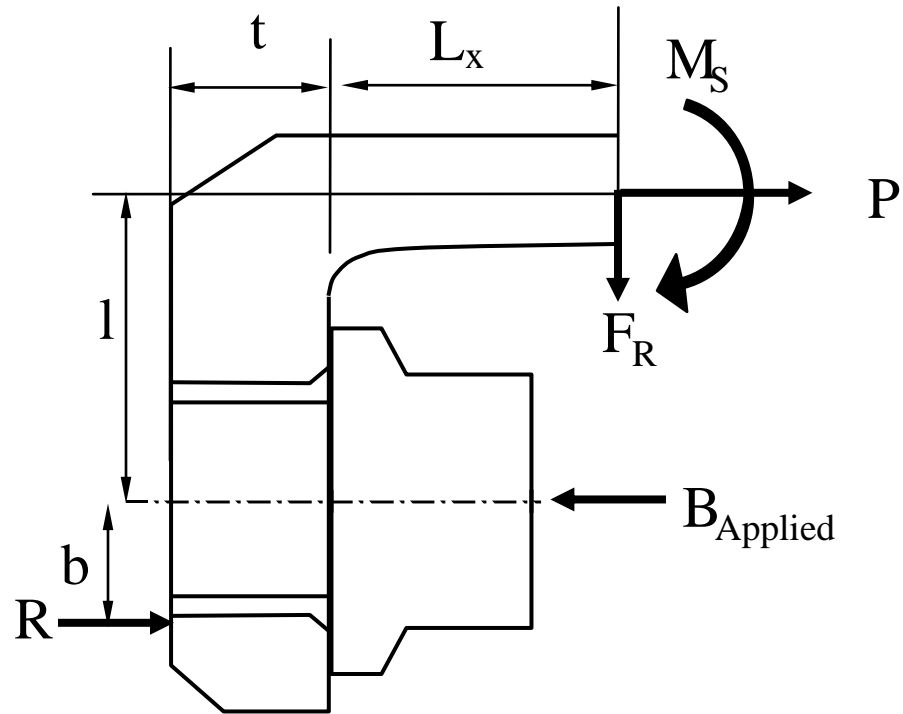


Figure 12: Example Joint Diagram (from [20])



Where,

$t$  = Flange thickness

$l$  = Radial distance from bolt centerline to applied shell load

$b$  = Radial distance from the bolt centerline to the toe reaction

$L_x$  = Axial distance from flange to the applied shell load

$R$  = Toe reaction

$M_s$  = Moment at shell

$P$  = Plug load at shell

$F_R$  = Radial load at shell

$B_{Applied}$  = Applied bolt load

Figure 13: Free Body Diagram for the Joint and Nozzle Support

## **CHAPTER 3**

### **ORIGINAL ANALYSIS**

#### **3.1 2D FEA METHODOLOGY**

Recent work completed to better understand the original nozzle support design was done using a 2D ANSYS® model. Geometry generated to represent the nominal part configuration was analyzed with Unigraphics NX4. Unigraphics is a computer aided design (CAD) suite of software from the Siemens Corporation used in digital product development and component modeling. This CAD technology is widely used in the automotive and aerospace industries to design and create digital drawings for complex components. This geometry was then imported into ANSYS®, and analyzed in the software suite's structural mechanics computer aided design tool. For the nozzle support, diffuser flange, and seal this software provided an exact model of the nominal hardware in two dimensions as shown in Figure 16.

This model is axisymmetric. Components shown are 2D representations of full 360-degree parts. Colors applied represent differences in material properties. For the basis of this model, the 2D representation assuming cyclic symmetry is adequate. Concerning applied loading, the combustor case shell is truncated just aft of the flange. This provides a location to apply fixities as well as loading from the case. Similarly, a combustor liner attachment is shown connected to the nozzle support. Although this attachment does not impart significant loads into the hardware, it is modeled here for completeness. The nozzle interface is also included so that nozzle loads may be applied to the hardware directly. These interfaces are important in proper modeling of the joint.

The coordinate system for this analysis is also important. This paper will refer to axial stresses along the engine centerline (y-axis), radial stresses (x-axis), and stresses in the hoop direction circumferentially around the engine (z-axis and axis of rotation for the 2D model).

### 3.2 ANSYS® ELEMENTS AND MESHING

The current model was constructed using PLANE25, axisymmetric, harmonic structural solid elements. Use of these elements is necessary as the nozzle loads impart translation in the axial and radial directions as well as rotation about the z-axis. PLANE25 elements have four nodes each. Nodes are capable of translation in the x, y, and z directions.

Bolts were modeled with BEAM3 elements. Again, this element type allows for three degrees of freedom necessary for this analysis. Both nodes in the element are capable of translation in the x and y directions as well as rotation about the z axis. The BEAM3 elements represent 2D elastic beams and areas. Material properties are set to match those of the bolt shank, head, and nut. These elements may also represent any cross-sectional shape for which the moment of inertia can be computed. This is a simple calculation for the bolt and nut in question. Assuming the bolt head, shank and nut act as cylindrical beams in the model we can calculate the direct and bending stress for each with the following equations.

$$A_{bolt} \cdot N_{bolt} = H_{Model} \cdot T_{Model} \quad (10)$$

$$N_{bolt} (\pi D_{bolt}^4 / 64) = (T_{Model} \cdot H_{Model}^3) / 12 \quad (11)$$

For simplicity we may note that the bending stiffness in the bolt head and nut need not be considered since any bolt bending will occur in the shank. In the above relations, the H and T refer to the radial height of each member and the circumferential thickness, respectively. For our model, the height and thickness of the modeled bolt, shank, and nut were equivalent to the actual part geometry. The areas of the bolt, shank, and nut are simply the cross sectional areas of the cylinders they make up and N is the number of bolts in the joint. Solving the above equations for the terms of interest we find the following for our real constants:

$$H = \frac{\sqrt{3}}{2} \cdot D \quad (12a)$$

$$T = \frac{\pi D \cdot N_{bolt}}{2\sqrt{3}} \quad (12b)$$

These real constants are applied to the model to accurately account for the stiffness of the bolts. These elements are limiting however, since their representation of stresses and their thermal gradients are assumed linear. For this model, the bolt head beam is coupled axially to the flange nodes. One node of the bolt head beam was coupled radially to one node of the flange to prevent free body translation of the bolt. The same is true for the nut. The bolt head, shank, and nut are also coupled in all three directions. In the joint of concern, there are 56 bolts. Forty-eight of the bolts are short bolts that connect directly to the nozzle flange. The eight other bolts are longer and connect to the flange through a bolt shield designed to protect the other bolts and minimize losses in the cavity. These long and short bolts are modeled separately using 2D point-to-point contact elements, CONTAC12, at the intermediate flanges, interference regions and gap locations. The nodes in the contact elements are coupled in the hoop



direction to prevent sliding. CONTAC12 elements are typically used with plane elements since the degrees of freedom they allow are consistent [23]. The methodology used to define the bolted joint is detailed in Figure 17.

For the mesh, special care is taken in creating and sub-dividing areas in the joint. Fillets, interface matching, transition areas and bolt holes are regions of interest that required special attention. Experience has shown that certain guidelines are essential to adequate modeling. Mesh densities are typically increased around key features such as fillets, element aspect ratios are monitored to reduce inappropriate bending, Gauss points are kept close to the surface and triangular elements are avoided whenever possible in agreement with the ANSYS user manual for the element type. Also, the mechanical mesh is matched as closely as possible to the thermal mesh. Although this can be difficult given the different requirements of the two models, this is usually well coordinated to guarantee proper temperature and pressure mapping.

### 3.3 BOUNDARY CONDITIONS AND APPLIED LOADS

In order to ensure proper joint behavior under the defined loading, several constraints were used. The forward end of the model is constrained in the hoop and axial directions at one node of the cut arm of the combustor case. This ensures no out of plane displacement and provides an axial fixity to the model. Loads derived from a separate combustor case model were also applied to the forward end to account for bending in the shell imparted by the case. These loads are visible in Figure 18. The aft end of the model was also critical. Loads resulting from the nozzle interface and combustion liner attachment were applied as shown in Figure 19.

The aft end is most significant as the substantial loads applied to the pinned joint have a considerable influence on the joint in question. Hot gasses exiting the combustion chamber and impinging on the nozzle impart a significant plug load on the hardware. This plug load is transferred from the nozzle to the aft support via a pinned joint. The aft support then passes this load on to the forward support as shown below. The result is a considerable eccentric load on the bolted joint. Forces on the combustor liner are generally not significant although they are included in the model for completeness. Pressure loads are also applied all around the shells modeled. These pressures are determined from separate Patran™ models used by secondary flows engineers and will be discussed in following sections of this paper. Figure 20 shows how the nozzle plug load is applied.

Loads for the model are scaled with the pressure at the compressor exit since nozzle loads correlate directly with these values. In this way, loads are ramped up and down throughout the mission according to their source pressure. A typical pressure mission map is shown in Figure 21. Note that pressures increase most dramatically during takeoff as the aircraft comes up to power quickly. This is typically the leg of the mission that is most severe and often the highest point in the LCF major cycle. Note too that flight maneuvers may also exist as the aircraft bursts and chops between steady state conditions. These maneuvers are often defined by the airframer and typically make up minor LCF cycles. Another significant point in the cycles is thrust reverse. This occurs during landing as the pilot commands the thrust reversers to redirect engine fan air forward to help rapidly slow the aircraft. This often results in a complete reversal of stress in core hardware and marks the low point in the LCF major cycle.

Since pressure in the area of concern parallels core speed, the chart in Figure 21 closely matches the typical commercial engine mission plotted as engine fan speed vs. time in Figure 22. Here again we see significant fluctuations in core speed at takeoff, thrust reverse and during flight maneuvers. Just as before, the major and minor LCF cycles clearly stand out. One could create a similar plot for engine temperatures in the core revealing the fluctuations that closely matched those in pressure and core speed. This gives a good sense of the conditions core hardware is subjected to.

For the basis of this analysis we concern ourselves primarily with the points surrounding takeoff and thrust reverse, the acceleration and deceleration points that typically define the major fatigue cycle. During each flight there is usually one major cycle from lightoff to maximum power and return to shutdown. In the case of this hardware it is the pressure cycle that is the most damaging. Other partial cycles cause additional damage depending on their associated mean and alternating stress levels. Although these are always included in hardware life cycle analysis, they are not as scrutinized as the major cycle. Of the hundreds to thousands of time points listed for an engine mission, time points surrounding the major cycle are examined more closely together. Often, time increments around takeoff differ only by hundredths of seconds. Proper fidelity is a must for the major cycle since it is typically a combination of temperatures and pressures that prove most detrimental. The entire range of data must be screened to ensure all possible damaging time points are selected for analysis. Limitations of FEA computation require the selection of specific time points. Since it would take weeks to iterate solutions for the entire mission and file sizes would be unmanageable, time points are chosen based on pressure differentials and temperature

gradients in key areas that define the major and significant minor cycles. The time points that contain the maximum pressure across the nozzle support shell and largest gradient through the joint of concern are examples of time points that would be chosen.

For hot structures like the nozzle support, thermal effects can play an important role. These effects can impact each critical location in a different manner, making the stress cycle more or less severe depending on the conditions. Experience on similar hardware in particular locations helps guide the cycle selection. Before the mission is defined in the analysis however, it is imperative that the model be set up correctly.

The first step in mechanical analysis is the achievement of preload. Preload in the joint is attained in the bolt through sequential assembly. First, preload is reached without friction to simulate assembly of the joint with lubricant. Then, friction is applied and the mission time points begin. The use of beam elements with stiffness calculated to represent the bolt allows it to behave in a realistic manner. To achieve preload, an initial interference is set as defined by the real numbers assigned to the contact elements under the nut. This value is generally determined through iteration and represents the bolt load applied to the joint. An initial interference is set, friction is removed, and the model is solved. Bolt loads are then checked against desired preload, taking into account the number of bolts in the application. The interference is then varied until the solution and desired result are well matched. The preload set in the initial condition is shown in Figure 23. Note that the stress distribution in the flanges closely matches that depicted in Figure 9 described earlier. The lines of constant stress in the clamped members, flanges, are strikingly similar to those predicted in Bickford's text. Since the bolt and nut are represented by beam elements, they do not appear in the figure below.

### 3.4 MATERIAL PROPERTIES

The forward nozzle support is made from industry standard Inconel 718 along with the diffuser. The aft nozzle support is Waspalloy as is the nut in the joint of concern. The seal flange is a lower alpha Inconel alloy and the bolt is standard MP159. Isotropic material properties are used throughout the model except at the bolt holes. In those locations, reduced orthotropic properties are used. Orthotropic areas are non-axisymmetric areas such as bolt holes, dovetails, scallops, etc. that must have their 3D stiffness accurately accounted for in the overall 2D model. This is commonly accomplished by modifying the stiffness of elements in those areas as defined by their material properties within ANSYS®. The modified stiffness can be calculated using other finite element models or using approximation techniques. In general, orthotropic elements are only used to adequately model the stiffness of an area. Stresses are often not representative of actual hardware. Care is also given to ensure material properties around cut outs and bolt holes are appropriately modeled. Reduction factors are calculated and applied where orthotropic properties are necessary. This allows analysts to correctly account for differences in elastic modulus, Poisson's ratio, coefficient of thermal expansion, etc. for three-dimensional features in a two-dimensional axisymmetric model. Although stresses in the areas of orthotropic material may be inaccurate, the elements surrounding these materials would be very representative of actual hardware. For areas where holes are concerned, a 3D sub-model is usually created. Although beyond the scope of this paper, sub-models are often used to complete the joint design.

Material properties were also specified for the CONTAC12 elements to account for friction. A specific coefficient of friction was used between flanges and at rabbet

interfaces while another, lower coefficient was used under the bolt head and nut to account to assembly lubricants. The coefficients may be varied to determine impact to the model and results.

At all locations material properties are considered minimum as derived from statistical analysis of material curves. The curves include average properties based on testing and  $-3\sigma$  or 99/95 properties. These are reduced properties to account for variance in material condition. The  $-3\sigma$  is simply three standard deviations below the average curve and the 99/95 curve is a statistical curve based on 99% exceedance of a 95% confidence band. The use of reduced property assumptions further ensures that design intent is met through conservatism.

### 3.5 HEAT TRANSFER ANALYSIS

From a thermal standpoint initial analysis begins with steady state conditions. Temperatures are noted at ground idle, climb, cruise, descent, etc. As the design evolves, transient temperatures play a vital role. In the case of the nozzle support and most bolted joints, thermal transients create a significant gradient in the joint as the inner and outer diameters heat up and cool down faster than the larger mass at the bolt centerline.

A complete thermal model is properly aligned with the stress model so that nodes are distributed according to the potential for high local thermal gradients and heat flow characteristics. For that reason, heat transfer analysis is conducted in much the same way solid modeling is done. Critical time points are chosen and known air temperatures and pressures are extracted from the mission cycle information. Performance engineers with selected operating conditions develop this mission cycle information. These

temperatures and pressures are combined with known flow values. A comprehensive and complex flow model is created. Due to the proprietary nature of these models, they will not be shown here. The flow model takes into account temperatures, pressures, and swirls inside cavities. A deflection solver is also used with given temperatures, coefficients of thermal expansion, and mechanical loads to calculate clearances between internal stationary and rotating seals. Heat transfer and secondary flow models are complex and their generation is beyond the scope of this paper. More explanation of heat transfer methods and programs is given in section 4.3.

The heat transfer model is much like the stress model. A mesh is created to match that of the stress model and heat transfer coefficients are applied where appropriate. The mesh is usually very coarse and not suitable for use in a stress model; however, key areas are given more attention. For example, bolted joints and important interfaces have a much higher element count than shells and simple, revolved features.

It is important to note that the heat transfer model is created in Patran™ and imported into ANSYS® for use in the stress model. Use of different pre-processors creates an inherent mismatch of meshes and models. Again however, this mismatch is understood and minimized as much as possible. For the model, material properties are set to yield appropriate conductive and density properties. Convection coefficients are applied to the surfaces of all members and contact between members is determined with set elements. For this analysis appropriate material identifications are applied to the bolt, nut, and joint members to achieve the proper behavior. The flows are modeled with the Flow Network Solver (FNS) fluids analysis software from TES Advanced Engineering Solutions that works with ANSYS®. The flow network solver with internal YFT solver is

a computer program used for analysis of steady state compressible fluid flow through networks of flow conduits and was created for use in the design of gas turbine engines. This software gives engineers the capability to model flow in rotating and static reference frames and also allows the transfer of fluid between these reference frames. These YFT networks consist of flow conduits or elements connected between nodes. Boundary chambers having fixed fluid properties define the boundaries of the network. Flows are then able to pass into or out of this network through associated boundary elements. These are highly complex models that take into account air constants, properties, and assumptions that help define temperatures and pressures along the members. Primary and secondary flows are modeled as well as radiation, convection, and conduction. Once complete, the heat transfer model is read into ANSYS<sup>®</sup> and overlaid on the structural model. In this way, pressures and temperatures from the flow model are applied to the geometry of the ANSYS<sup>®</sup> model in a consistent manner. It is important to point out here that the heat transfer model treated the flanges as tightly clamped throughout the mission and included high convective coefficients at the interfaces. Leakage therefore, was assumed to be insignificant and flange contact at the outer diameter was modeled involving conduction rather than convection. This is an important assumption in flange leakage and flow analysis.

The heat transfer model used for this analysis was originally created in the early 1980s and, like the stress model, has evolved over time with advances in modeling. In addition to technological capabilities, these models have been updated to fully depict the actual engine architecture as it exists today. Design changes incorporated through cost reduction, process improvement, and the advancement in manufacturing capabilities have



been fed back into the model to determine their impacts. Further, extensive engine tests spanning decades have allowed engineers to remove some of the conservative assumptions initially made. One such assumption amended by engine testing is the values of  $h$ , or heat transfer coefficient, used throughout the heat transfer model. The selection of heat transfer coefficients is usually based on past engine test data correlated to analytical models to arrive at reasonable values. Based on this test data correlation, multipliers are generally added to the heat transfer coefficients in the model at various locations. These  $h$  multipliers increase the rate at which material responds to changes in temperature. High  $h$  values attached to a material will make it heat up or cool down more rapidly. In sensitive areas like bolted joints this can cause artificially high gradients, leading to increased thermal strain and reduced low cycle fatigue life. For flows around the hardware of concern, inner structure hardware, an  $h$  multiplier of  $Y$  is generally used based on historic data. Just as before, actual values are replaced with symbolic representations due to the proprietary nature of the data. Heat transfer coefficients at the nozzle support interface however, were revised following engine tests conducted in the mid-1990s. These  $h$  multipliers were increased to  $2Y$  to match thermocouple readings taken at the flange's inner diameter, outer diameter, and bolt hole. An  $h$  multiplier of  $2Y$  would force hardware to heat up twice as fast as an  $h$  multiplier of  $Y$ .

Although analysis correlated to test data is usually the best approximation for actual engine conditions, there are several understood instrumentation limitations in terms of accuracy and longevity. These limitations can dramatically impact the verification results. Efforts are generally made to obtain duplicate readings across a wide array of thermocouples. This distribution provides a complete set of thermocouple data

and engineers can be confident about the resultant thermal description of the hardware. For that reason the latest engine test required several thermocouples to be placed in each location at the nozzle support flange inner diameter, bolt hole inner diameter, bolt hole outer diameter, and flange outer diameter. This gave a full radial temperature profile of the joint. In critical locations, multiple readings are desirable, and thermocouples are usually placed at several o'clock positions around the component. This requirement must sometimes be weighted against test facility limitations, instrumentation requirements of other hardware, cost, and schedule. This can sometimes limit the overall number of desired readings. Several o'clock locations were chosen and a number of thermocouples were placed for redundancy. Although great care was taken to properly distribute thermocouples and the current models are correlated to that data, the need of an  $h$  multiplier of  $2Y$  in place of the usual  $Y$  necessitates further analysis to fully understand temperature readings at the joint of concern. Since the  $h$  multiplier is twice the typical factor, heat transfer engineers have recently questioned the accuracy of the thermocouples and whether they measured air, metal or some combination of air and metal temperatures. Future tests will focus on this area for improved fidelity of the temperature profile.

### 3.6 STRUCTURAL ANALYSIS AND LCF LIFE CALCULATIONS

Running the solution for the above model we note stresses at two critical time points in the defined mission loading. Although the mission analyzed contained dozens of time points, we only examine two for the basis of this paper. One time point during takeoff and one during landing (thrust reverse) are considered for the major LCF cycle.

Plots for hoop stress, axial stress, equivalent or Von Mises stress, and temperature are shown in section 3.7, Figures 25-32. Here again scales have been removed. Note that all areas of stress concentration align with engineering judgment. Axial plots clearly show flange bending as indicated by higher tensile stresses in fillets and hoop stresses align with Bickford's texts. Note too the temperature plots which show significant thermal gradients, primarily at takeoff. Although the scale as been removed a significant temperature difference is evident. Radial stresses are insignificant to this bolted joint and, although included in LCF life calculations, are not presented here.

In order to determine LCF life for the flange in question, we follow simplified, technical literature regarding stress concentration and analysis methodologies. In fact, the analytical approach used here is typical in the aerospace industry where cyclic stresses are high enough to cause cracking. First, stresses for the entire mission are pulled from the model at the four locations representing the forward inner, forward outer, aft inner and aft outer diameter points of the bolt hole as shown in Figure 33.

Next, bolt hole stress concentration factors are determined. These stress concentration factors (Kts) may be determined from Peterson's text on stress concentrations [24]. These stress concentrations must be applied to the appropriate components of stress defined by the model. Stresses are first broken down into their tensile and bending components using the following relationships.

$$\text{Meridional Tensile Stress (S}_{x_{\text{tensile}}}) = \frac{(S_{x_{\text{nodeA}}} + S_{x_{\text{nodeB}}} + S_{x_{\text{nodeC}}} + S_{x_{\text{nodeD}}})}{4} \quad (13)$$

$$\text{Meridional Bending Stress (S}_{x_{\text{tensile}}}) = \frac{\left( \frac{(S_{x_{\text{nodeA}}} + S_{x_{\text{nodeC}}})}{2} - \left( \frac{S_{x_{\text{nodeB}}} + S_{x_{\text{nodeD}}}}{2} \right) \right)}{2} \quad (14)$$

$$\text{Hoop Tensile Stress } (S_{z_{\text{tensile}}}) = \frac{(S_{z_{\text{nodeA}}} + S_{z_{\text{nodeB}}} + S_{z_{\text{nodeC}}} + S_{z_{\text{nodeD}}})}{4} \quad (15)$$

$$\text{Hoop Bending Stress } (S_{z_{\text{bending}}}) = \frac{\left( \frac{(S_{z_{\text{nodeA}}} + S_{z_{\text{nodeC}}})}{2} - \left( \frac{S_{z_{\text{nodeB}}} + S_{z_{\text{nodeD}}}}{2} \right) \right)}{2} \quad (16)$$

$$\text{In-Plane Bending Stress } (S_{z'}) = \frac{\left( \frac{(S_{z_{\text{nodeA}}} + S_{z_{\text{nodeB}}})}{2} - \left( \frac{S_{z_{\text{nodeC}}} + S_{z_{\text{nodeD}}}}{2} \right) \right)}{2} \quad (17)$$

In the above equations,  $S_x$  denotes the axial component of stress and  $S_z$ , the hoop component at the respective nodes A, B, C, and D. Stress concentrations due to the bolt hole geometry are then applied in tension and bending for each direction so that they are specifically aligned to the proper component of stress. Bolt hole  $K_t$ s are applied according to the following equation for stress at the bolt hole bottom.

$$\text{Stress at C} = (K_{t_1} \times S_{z_{\text{tensile}}}) + (K_{tb_1} \times S_{z_{\text{bending}}}) + (K_{t_4} \times S_{x_{\text{tensile}}}) + (K_{tb_4} \times S_{x_{\text{bending}}}) + (K_{t_{1a}} \times S_{z'}) \quad (18)$$

In this case, stresses at node C are most severe. Stresses at the other nodes may be determined in the same manner. In the case of this bolted joint, engineering judgment and experience suggest that stress at the forward bolt hole bottom is most severe. In fact, for a complete analysis low cycle fatigue life is determined over the entire surface of the part. In this way, all key features are analyzed and bolt holes are fully examined. For this paper however, fatigue life is assumed to be lowest at location C from Figure 33. Taking into account bolt hole diameter, flange thickness, flange width, and bolt hole spacing one may generate  $K_t$ s for tension ( $K_{t_1}$ ,  $K_{t_2}$ ,  $K_{t_3}$ ,  $K_{t_4}$ ), bending ( $K_{tb_1}$ ,  $K_{tb_2}$ ,  $K_{tb_3}$ ,

K<sub>tb4</sub>) and in-plane bending (K<sub>t1a</sub>). The 1, 2, 3, and 4 refer to the locations around the bolt hole, 1 at 12 o'clock and 2, 3, and 4 offset 90 degrees from one another, clockwise, forward-looking aft. These K<sub>t</sub>s may be determined from Peterson's text using the geometry for the flange and bolt hole. This provides 3D stress concentrations for the 2D model.

With appropriate stresses and temperatures we may now consider low cycle fatigue life. Low cycle fatigue is usually considered to be failure in less than 10<sup>5</sup> cycles. High cycle fatigue (HCF), in contrast, occurs within the elastic range at lower stress levels and often involves high frequency. Like HCF, LCF involves some degree of plastic deformation although frequencies are generally much lower. Design for fatigue is normally based on one of these two failure modes together with consideration of the mean and alternating stress levels. For a given set of load conditions, the mean stress is the average of the maximum and minimum stresses, and the alternating stress is half of the difference between the maximum and minimum stresses during the operating cycle.

Several theories exist for determining low cycle fatigue life. Life calculations for structural aerospace hardware, like the nozzle support, generally adhere to the shear strain energy theory, which assumes constant elastic strain energy of distortion. The effective or Von Mises stress is identified as a measure of nearness to failure of a component. This stress should therefore be kept sufficiently under allowable stress levels defined by material curves and testing. The equation below represents effective stress in three-dimensional Cartesian coordinates.

$$2\sigma_e^2 = (\sigma_x - \sigma_y)^2 + (\sigma_y - \sigma_z)^2 + (\sigma_z - \sigma_x)^2 + 6(\tau_{xy}^2 + \tau_{yz}^2 + \tau_{zx}^2) \quad (19)$$

Here, the stresses,  $\sigma$ , and shear stresses,  $\tau$ , define the state of stress at any given point in time at any location on the hardware. Here again, x, y, and z are defined as radial, axial, and circumferential (hoop) direction, respectively. Shear stresses are defined along the planes on which they act. With the definition above we can then define the alternating and mean stresses for fatigue determination. The alternating stress in terms of the effective stress in three dimensions is then:

$$\sigma_{alt} = \frac{\sqrt{2}}{2} \left[ (\Delta\sigma_x - \Delta\sigma_y)^2 + (\Delta\sigma_y - \Delta\sigma_z)^2 + (\Delta\sigma_z - \Delta\sigma_x)^2 + 6(\Delta\tau_{xy}^2 + \Delta\tau_{yz}^2 + \Delta\tau_{zx}^2) \right]^{\frac{1}{2}} \quad (20)$$

Where,

$$\Delta\sigma_x = \sigma_{x1} - \sigma_{x2}$$

$$\Delta\sigma_y = \sigma_{y1} - \sigma_{y2}$$

$$\Delta\sigma_z = \sigma_{z1} - \sigma_{z2}$$

$$\Delta\tau_{xy} = \tau_{xy1} - \tau_{xy2}$$

$$\Delta\tau_{yz} = \tau_{yz1} - \tau_{yz2}$$

$$\Delta\tau_{zx} = \tau_{zx1} - \tau_{zx2}$$

Similarly, the mean stress is:

$$\sigma_{mean} = \frac{\sqrt{2}}{2} \left[ (\Sigma\sigma_x - \Sigma\sigma_y)^2 + (\Sigma\sigma_y - \Sigma\sigma_z)^2 + (\Sigma\sigma_z - \Sigma\sigma_x)^2 + 6(\Sigma\tau_{xy}^2 + \Sigma\tau_{yz}^2 + \Sigma\tau_{zx}^2) \right]^{\frac{1}{2}} \quad (21)$$

Where,

$$\Sigma\sigma_x = \sigma_{x1} + \sigma_{x2}$$

$$\Sigma\sigma_y = \sigma_{y1} + \sigma_{y2}$$

$$\Sigma\sigma_z = \sigma_{z1} + \sigma_{z2}$$

$$\Sigma \tau_{xy} = \tau_{xy1} + \tau_{xy2}$$

$$\Sigma \tau_{yz} = \tau_{yz1} + \tau_{yz2}$$

$$\Sigma \tau_{zx} = \tau_{zx1} + \tau_{zx2}$$

Aircraft components may also adhere to the Walker Mean Stress Model since they often operate with varying mean stresses due to the cyclic missions they are subjected to. Using Walker parameters, engineers are able to adjust stress levels to material test data in order to accurately predict hardware life. Key Walker parameters are defined below [25]:

$$R = \frac{\sigma_{\min}}{\sigma_{\max}} \quad (22a)$$

$$A = \frac{\sigma_{alt}}{\sigma_{mean}} \quad (22b)$$

These parameters, the A and R ratios, allow engineers to correlate actual component stress levels to those tested. Typically, A=1 and R=0 for standard tests. This stems from LCF testing during which the minimum stress is zero and the maximum stress is some value larger than zero. During testing, mean and alternating stresses are easily controlled. During the missions witnessed by aircraft engines however, mean and alternating stresses can vary widely. The equation below permits us to compare alternating stresses where A ratios may not equal one to test data where the A ratio was controlled. Here the  $\sigma_{alt}$  is a modified stress amplitude based on Walker parameters [25].

$$\sigma_{alt} = \frac{1}{2} \sigma_{\max} (1 - R)^m \quad (23)$$

Where m, the Walker exponent is an empirically determined parameter

For some aerospace applications other failure theories may be better suited for life determination. For the Inconel 718 nozzle support the strain energy theory is fitting. Mean and alternating stresses may then be compared to material curves for cycle damage determination. These curves, S-N diagrams, are generated from test data gathered over several years. The S-N diagram is a relation showing stress, in this case alternating pseudostress, and the number of cycles to failure for a given material at a certain temperature. Tests are conducted by alternating tensile and compressive loads on standard test bars where the maximum compressive stress equals the maximum tensile stress. The maximum amplitude of either stress is plotted on the vertical axis and the number of cycles required to fail the test coupon is plotted on the horizontal axis. The curve shows the mean life of the test coupons. Coupons differ drastically from one another so several tests are conducted for a good data set from which to form a statistical baseline. From the S-N curve we note that as alternating stresses are reduced, cycle life increases until virtually parallel with x-axis. This is called the endurance limit or reversing stress level below which fatigue life is infinite for all intensive purposes. An example S-N curve is shown in Figure 34.

It is a key point of detail that in this analysis alternating pseudostress is used. Here we assume that the strain distribution is unchanged by any elastic-plastic conditions. In this way, even though local stresses may exceed yield, the strain-controlled nature of the part assumes the overall behavior will be elastic. The relationship for pseudostress is given below.

$$\text{Pseudostress} = E * e_L \quad (24)$$

$e_L$  = Longitudinal strain



$E$  = modulus of elasticity

Without going into the mathematics behind the above relation, we will equate elastically calculated effective stresses to the pseudostress calculated from a standard smooth bar specimen. As noted earlier, we are also equating effective strains, which is appropriate for this strain-controlled joint. With life to crack initiation due to low cycle fatigue, one would typically move into fracture mechanics to determine the life to crack propagation. For this paper however, we will only address crack initiation since any cracking on this part in this area is unacceptable and cause for part replacement or repair. In general, a crack is said to initiate when an engineering indication forms. An engineering indication can mean different things depending on the application. A surface or corner crack is usually assumed to be certain size and analytically exists in the part after LCF crack initiation. This is usually consistent with the inspection capabilities required for the part. From the above equations and relationships we find X cycles to failure for the nozzle support. The term cycles, as used here, relates to the number of times the engine passes through the mission indicated earlier. The engine could be expected to survive X missions without failure in this location.

We may now use the Walker model to assess the influence of mean stresses on fatigue lives considering the full damage content for the defined mission through the use of a damage rainflow counting. For this paper a rainflow counting technique for a repeating history per ASTM E1049-85 may be applied. This technique ensures the magnitudes of alternating stress are properly accounted for. In fact, damage-counting software schemes can be used correctly identify the most damaging cycle based on the

stress and temperature data. A damage counting algorithm internally identifies the most damaging major cycle, for this hardware this consists of a fully reversed loading cycle between takeoff and descent. The most damaging major cycle is determined by evaluating every combination of mission points to find the combination that will produce the lowest life [26].

All subsequent minor cycles are then identified using the more traditional rainflow techniques. The damage rainflow method recognizes that LCF life is a function of both stress and temperature. To use this method, all the stress and temperature points are compared to one another. The combination of stress and temperature points that produce the lowest calculated LCF life is then regarded as the primary cycle. When cycle counting is considered, a cyclic sequence is constructed. The cycle is created such that it begins with the highest stress peak and continues through the stress time history until the highest stress time point is repeated. This defines the cycle for use in the rainflow counting. Starting from the highest peak, the program goes down the stress range to the first stress reversal and proceeds horizontally to the next downward range. It follows it down the stress range to the next reversal. This procedure is continued until the lowest stress point is reached. Once the lowest peak is identified, the program moves up the stress range to find the first stress reversal. The program then proceeds horizontally to the next upward range and follows it up to the next reversal. This procedure continues until the program reaches the repeated highest stress point. The highest and lowest stress points define the primary cycle. The stress time history above or below the horizontal lines represent additional secondary cycles that must be counted. In this way all cycles are accumulated for all sections of the mission.

An example of the application of this stress rainflow method is shown in Figure 35 for a typical stress time history. The complete mission is shown in the first figure and stress levels follow the pattern 1-2-3-4-5-6-7-8 returning to 1. Cycle counting per the methodology above shows the primary cycle, 1-4-1, beginning at the highest stress peak and moving down to the first stress reversal. The program then moves horizontally and continues downward to the next stress reversal. Since this marks the lowest stress, the program reverses direction, moving up back toward the highest stress. The program moves horizontally when it reached the intermediate peak at point 5 and continues up to the highest stress to complete the cycle. The second line of the figure shows the revised pattern with the primary cycle, 1-4-1 set aside. This primary cycle also divides two other patterns, 2-3-2 and 5-6-7-8-5. The arrangement 2-3-2 is a cycle in itself. The pattern 5-6-7-8-5 can be further broken down in to the cycles 5-8-5 and 6-7-6 shown on the third line. Each of these secondary cycles can then be considered in LCF analysis.

As discussed earlier, the LCF predictions made here are conservative over actual part life witnessed in the field. In the field, no cracking for fatigue distress is observed in the area of the nozzle support. The majority of the engines in the fleet have 3-4X cycles. Although several conservative assumptions are made in the determination of LCF life at this joint, one would still expect cracking. The primary reason the model seems to be predicting lower life to crack initiation is due to the thermal gradient on the nozzle support flange. A normalized plot of the gradient is shown in Figure 36. Note that the Delta Temp indicated in the figure represents the difference between temperatures at the inner diameter (ID) and outer diameter (OD) of the flange.

According to the above information, the heat transfer analysis and modeling is creating significant thermal gradients in the forward flange of the nozzle support. The high gradients predicted by the model, particularly noticeable during takeoff, seem to drive LCF life. No cracking is noted on fielded parts though; implying gradients are not as harsh as indicated in Figure 36. The model used for mechanical analysis couples nodes between the forward flange of the nozzle support and the combustor case and does not allow for flange separation and leakage. Again, the model is not accurately reflecting part behavior in service. For that reason, effort has recently been made to determine flange separation and leakage and apply those factors into the joint model.

### 3.7 FIGURES

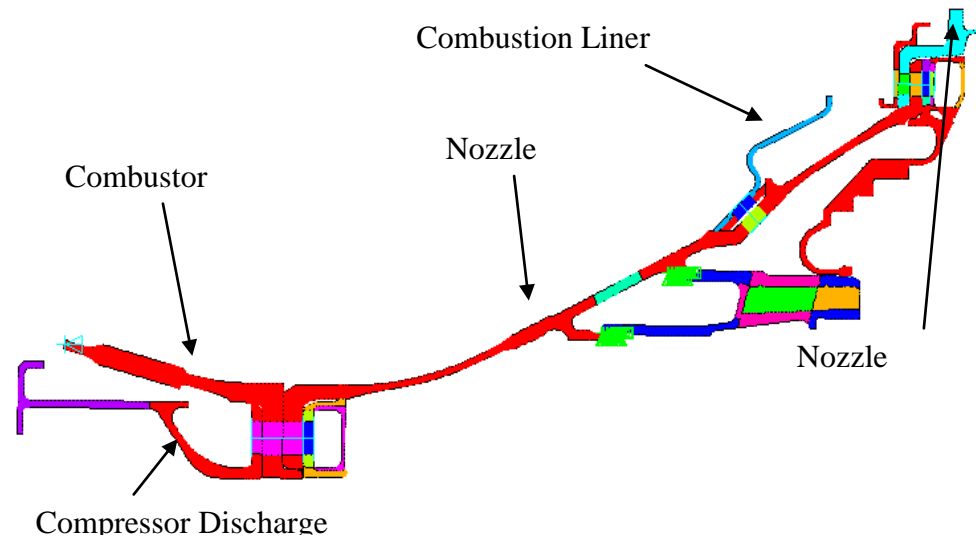


Figure 14: 2D ANSYS® Model

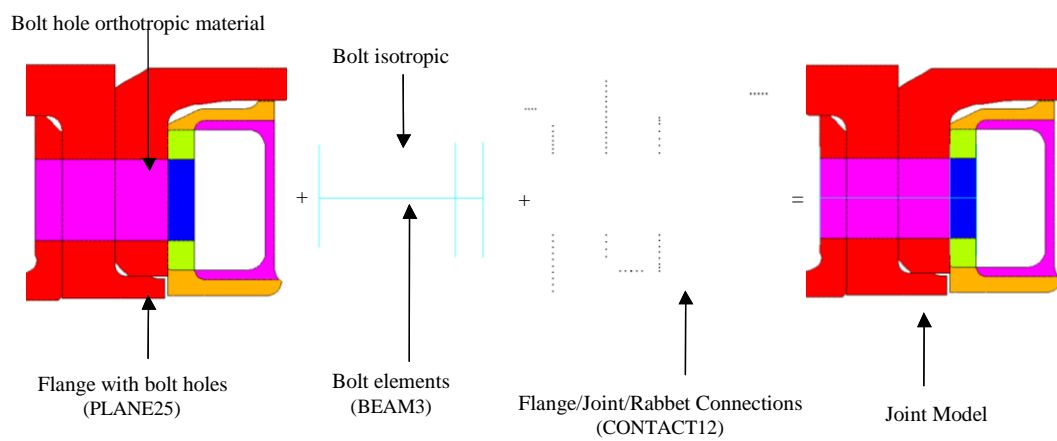


Figure 15: Bolted Joint Modeling

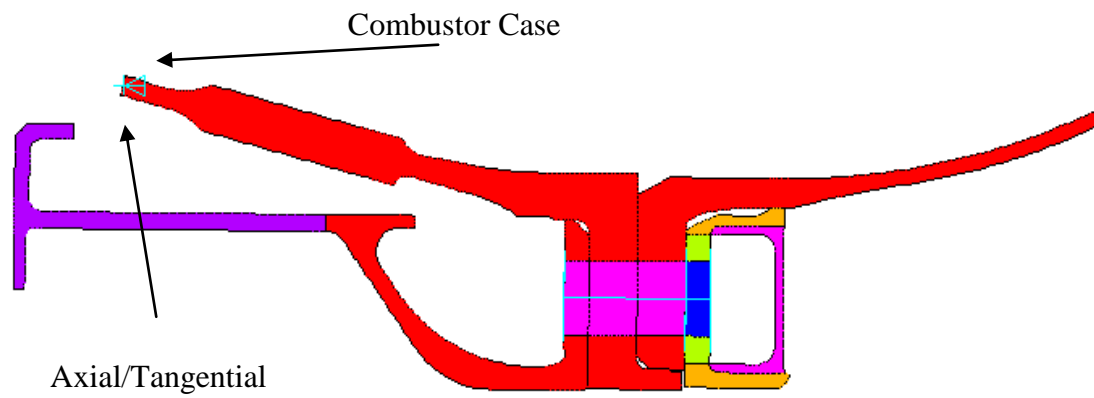


Figure 16: Model Forward Constraints and Loads

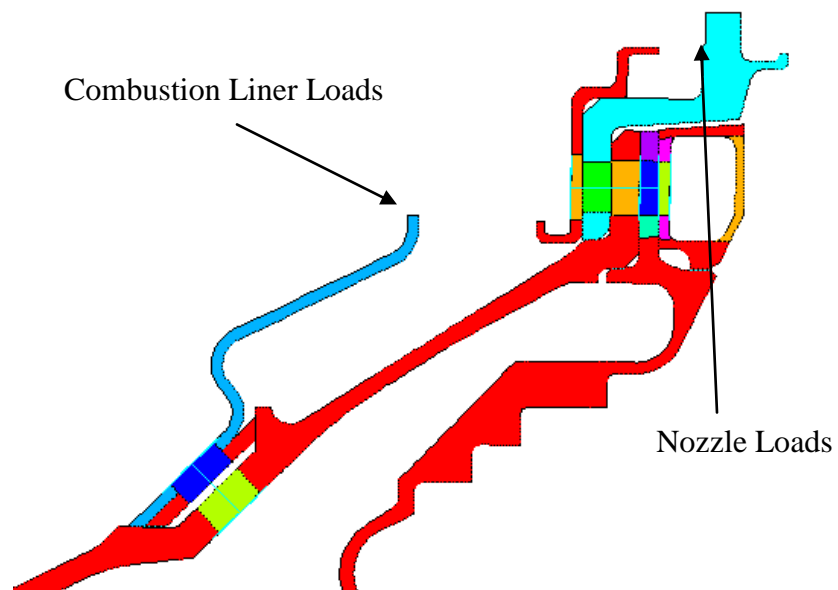


Figure 17: Model Aft Constraints and Loads

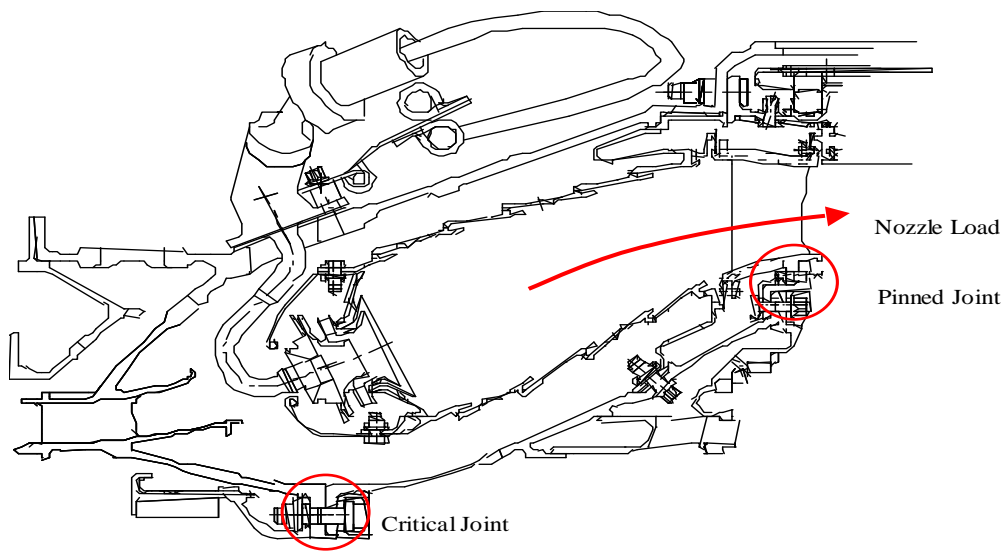


Figure 18: Nozzle Load Detail

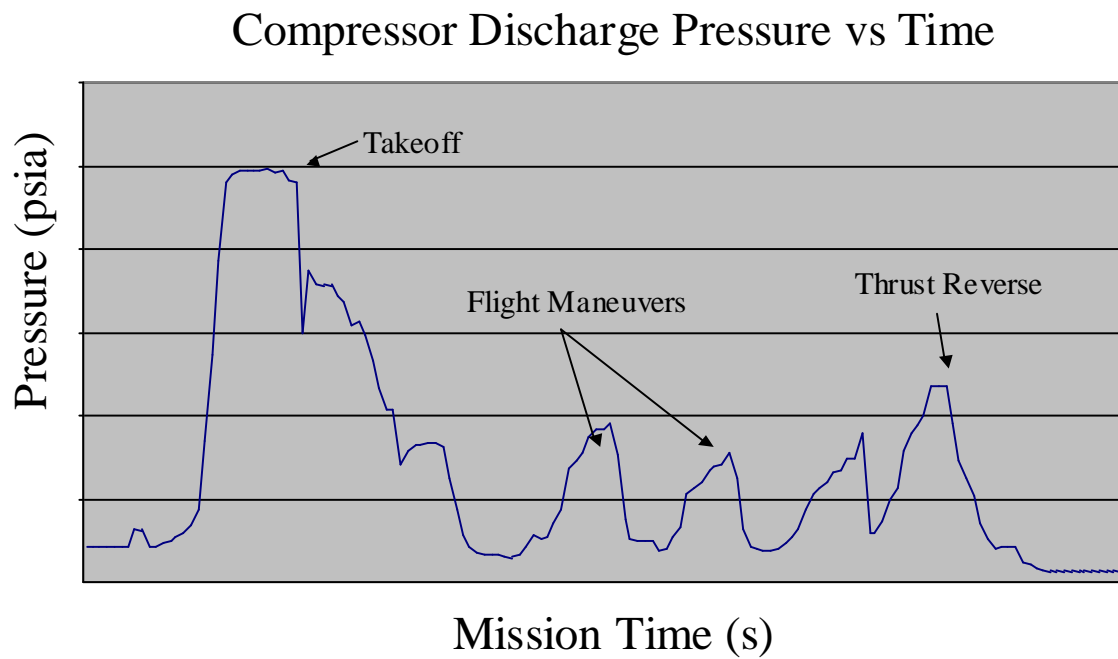


Figure 19: Mission Pressure Profile

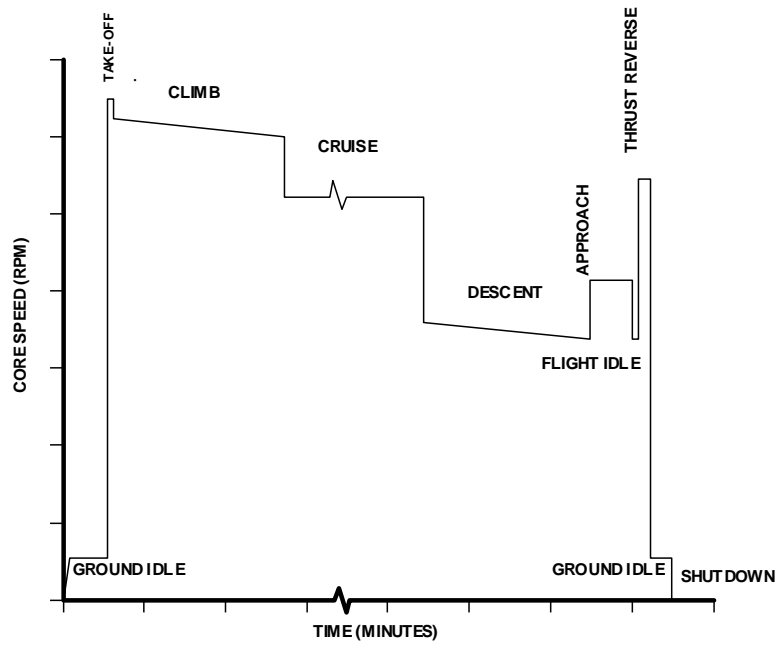


Figure 20: Typical Commercial Engine Mission

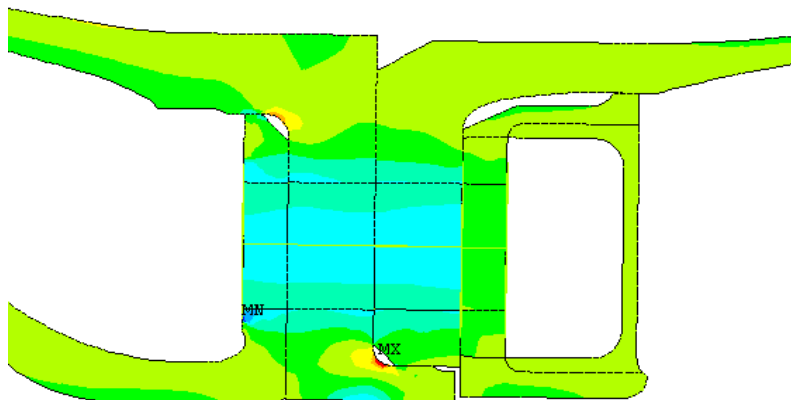


Figure 21: Modeling Bolt Preload



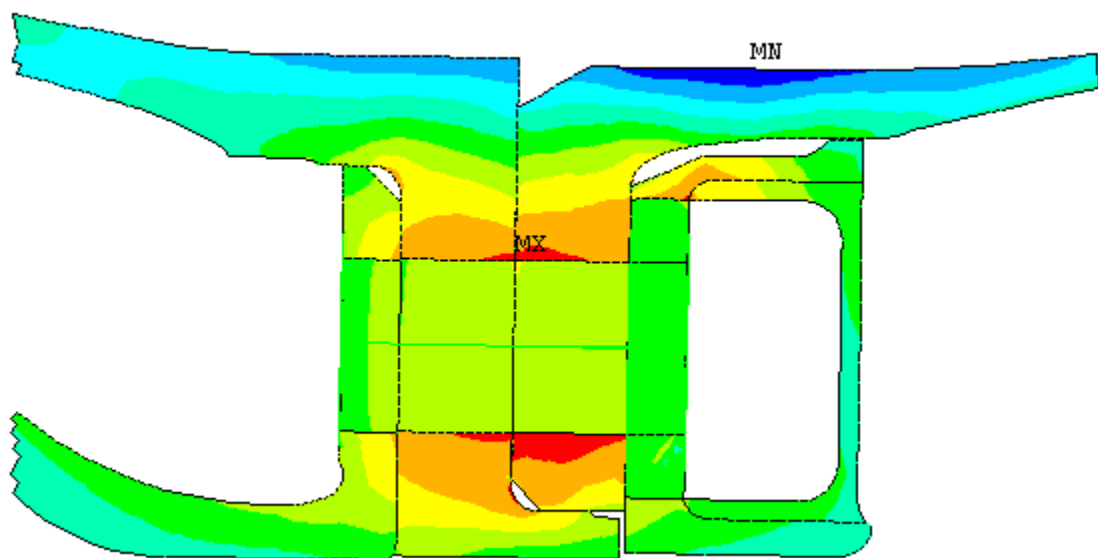


Figure 22: Hoop Stresses at Takeoff

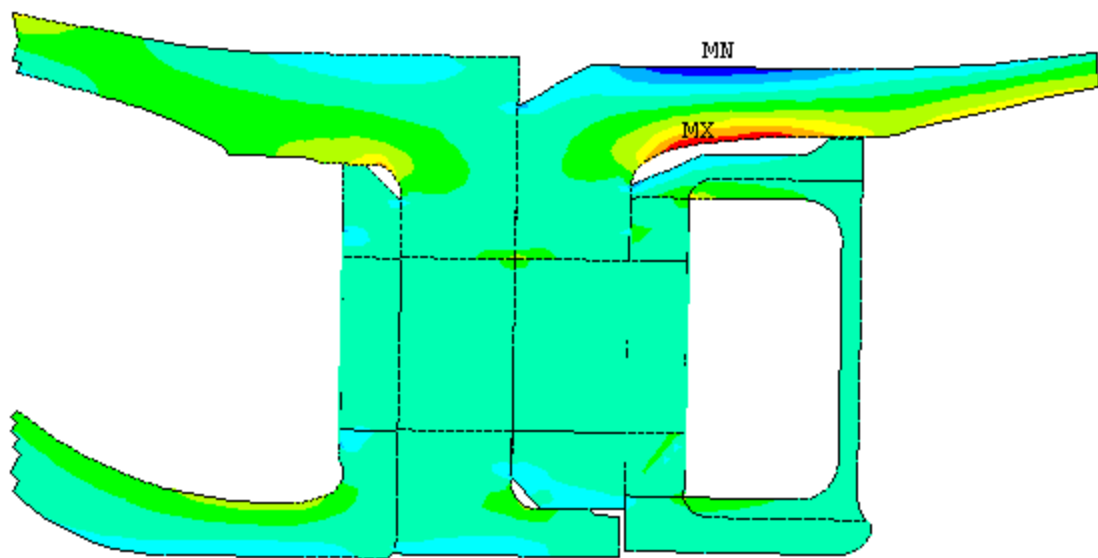


Figure 23: Axial Stresses at Takeoff

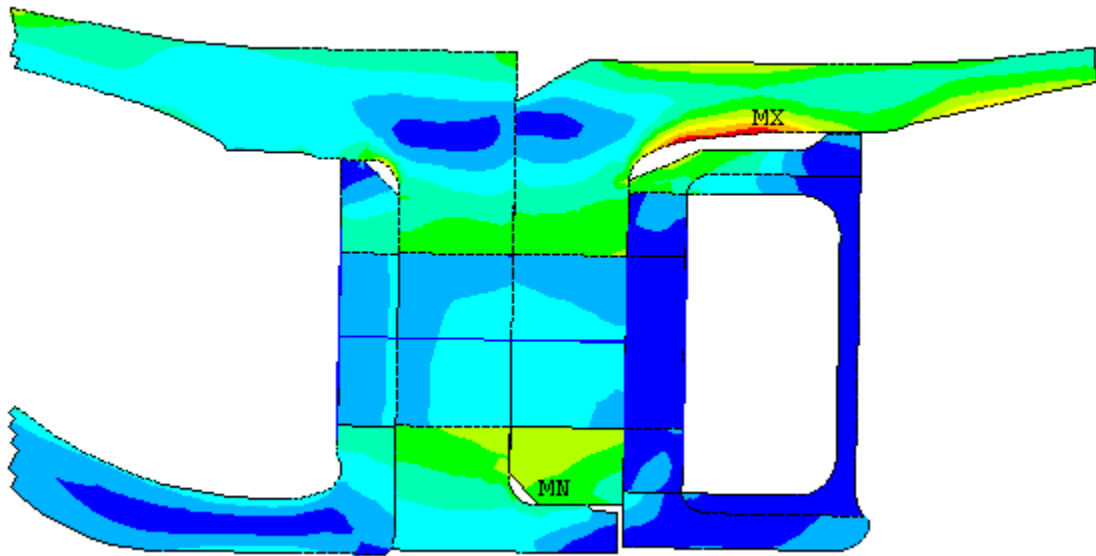


Figure 24: Equivalent Stresses at Takeoff

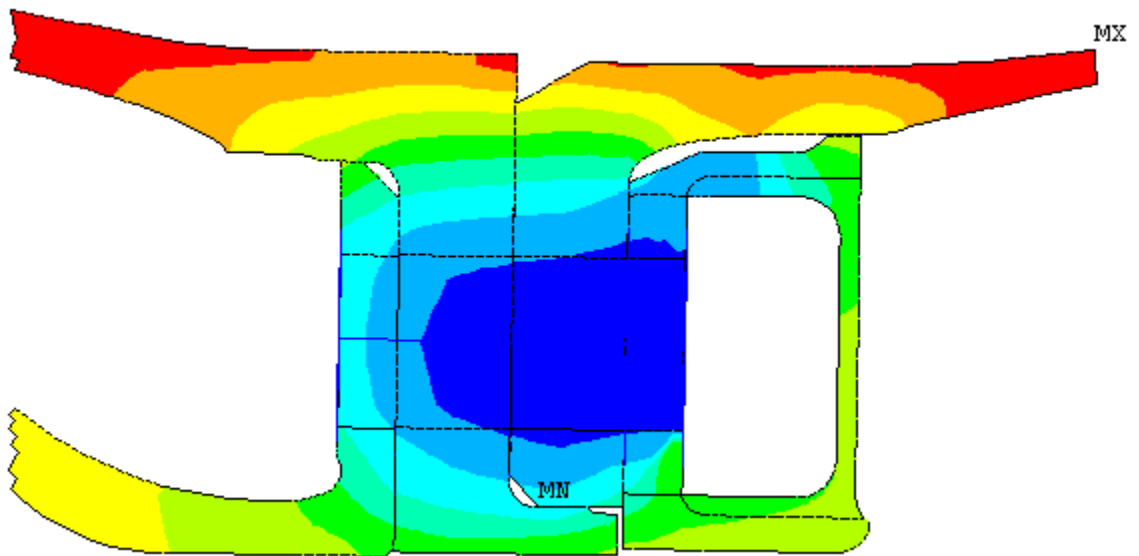


Figure 25: Temperature Distribution at Takeoff

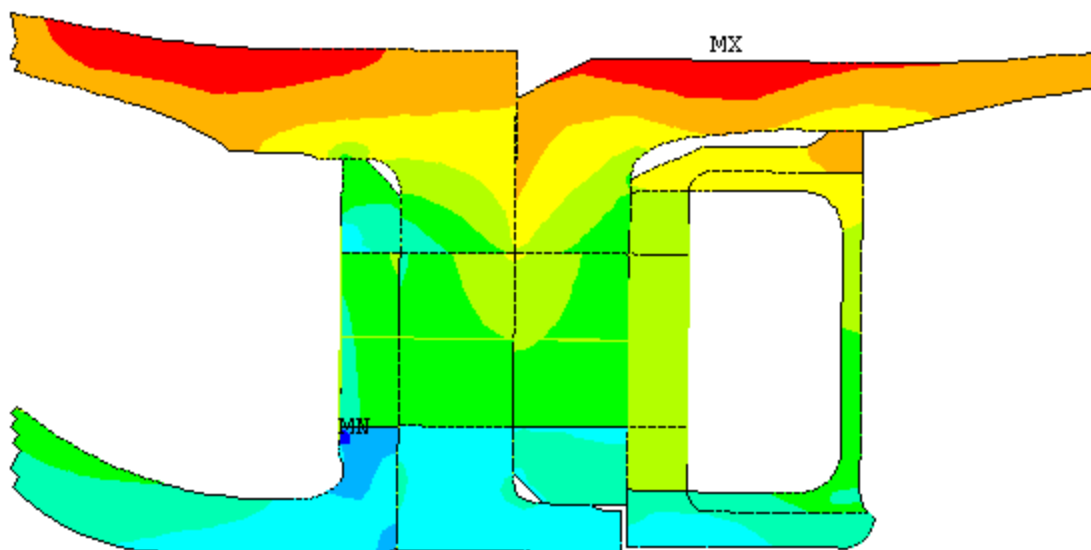


Figure 26: Hoop Stress at Thrust Reverse

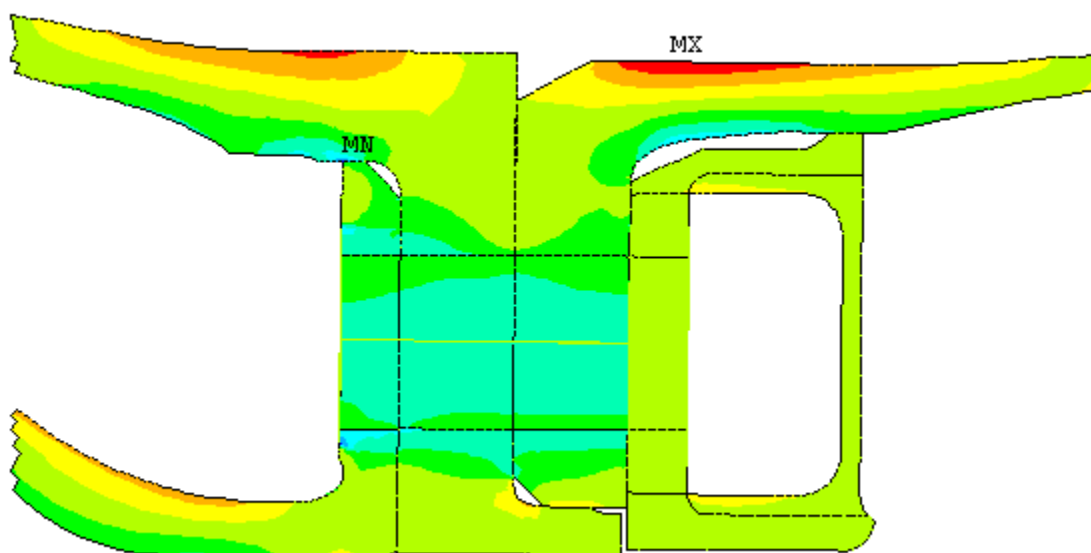


Figure 27: Axial Stress at Thrust Reverse

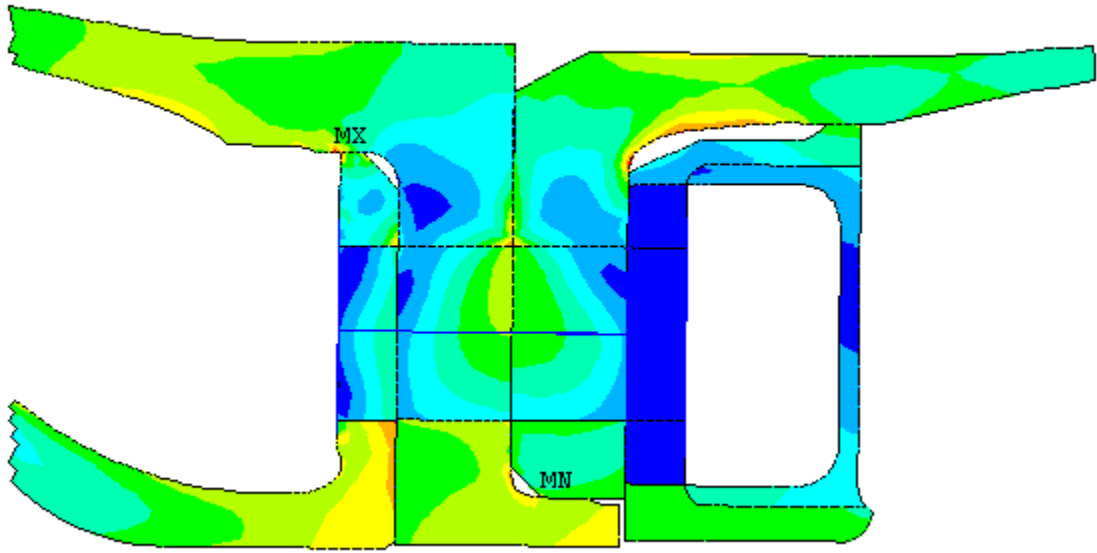


Figure 28: Equivalent Stress at Thrust Reverse

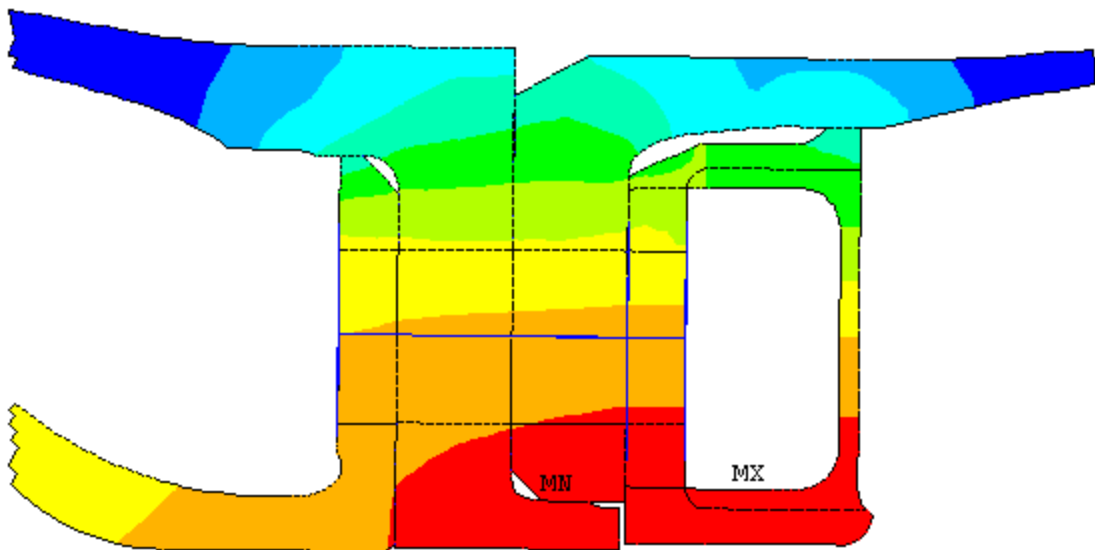


Figure 29: Temperature Distribution at Thrust Reverse

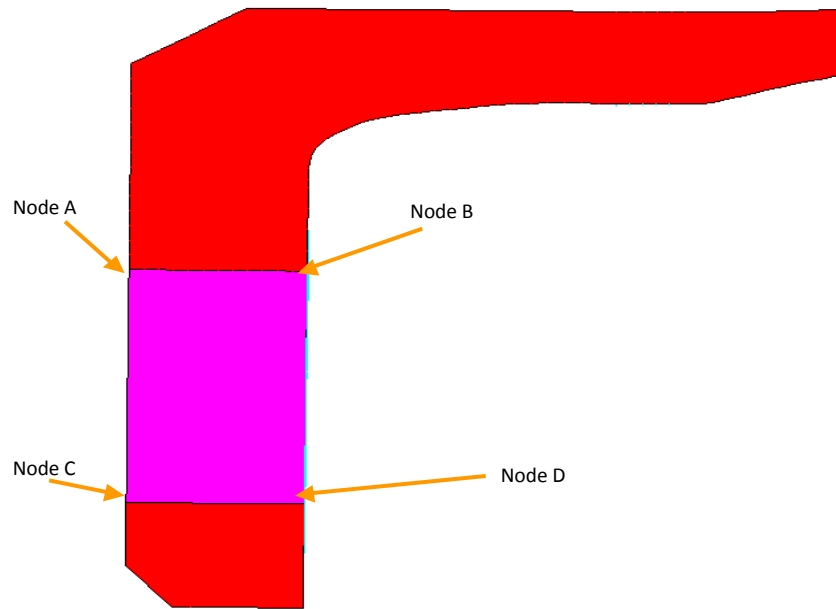


Figure 30: Bolt Hole Nodes Chosen for Life Calculation

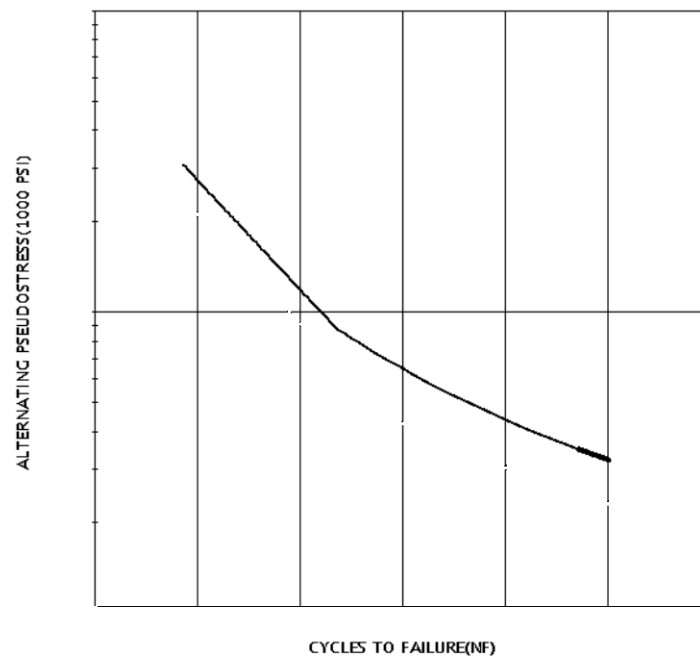


Figure 31: Example S-N Curve

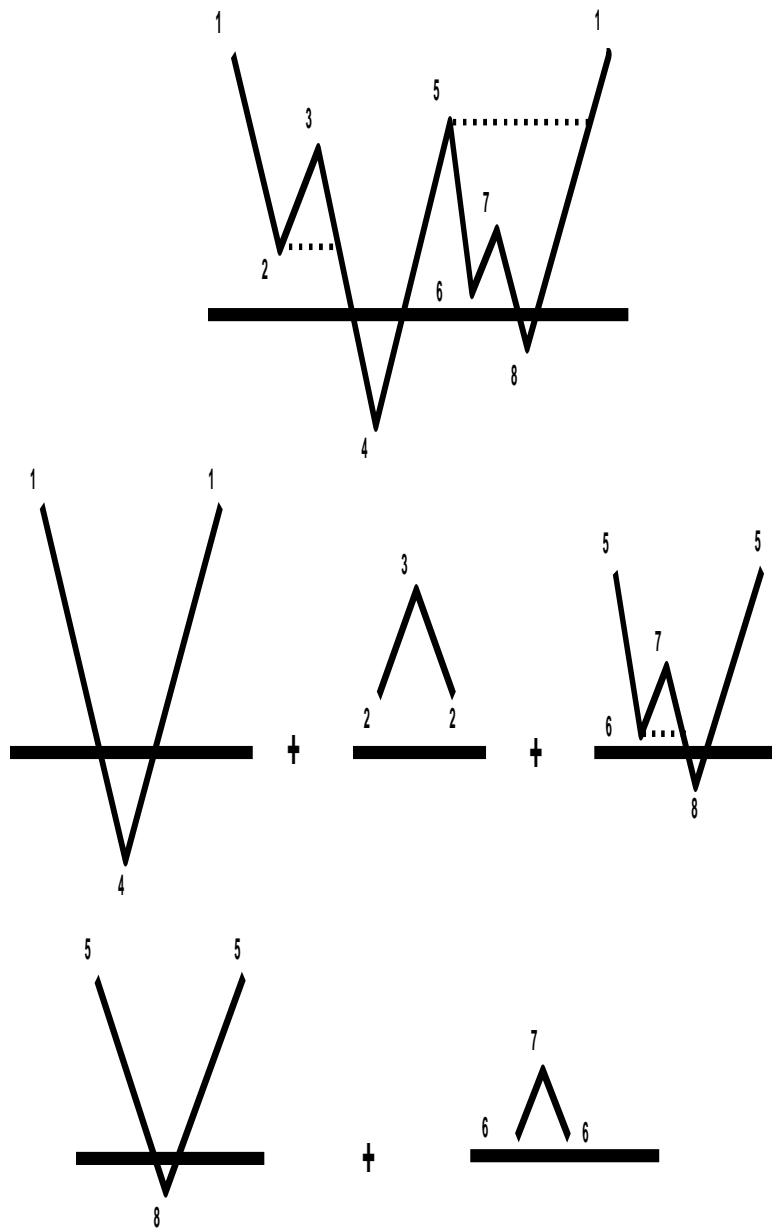


Figure 32: Example Rainflow Counting Procedure

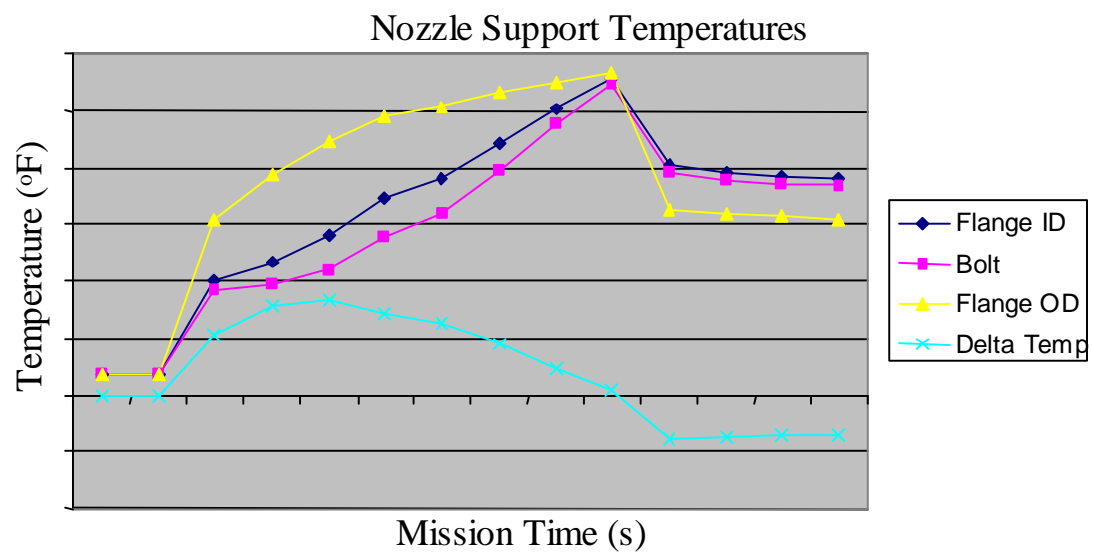


Figure 33: Nozzle Support Flange Temperatures vs. Mission Time

## **CHAPTER 4**

### **IMPROVED MODELING**

#### **4.1 2D FEA METHODOLOGY**

For the improved model, more realistic analysis methods were incorporated. Instead of the simplified 2D beam elements used earlier, SHELL43 elements were used for the bolt head, shank, and nut. Coincident nodes were merged to join the bolt and nut in the area of the threads. Real constants account for bolt component stiffness and geometry as was done with the beam elements previously. A thickness is set using the area moment of inertia and number of bolts. The use of shell elements instead of the rigid body elements used earlier gives several advantages. Temperatures can be applied to shell elements to reflect characteristics at the bolt shank, head, and nut. For 2D modeling, shell elements provide the most accurate representation of the actual hardware. The BEAM3 elements used originally used were uniaxial elements with tension, compression, and bending capabilities. They were limited in that they only allowed for three degrees of freedom at each node, translations in the nodal x and y directions and rotation about the nodal z-axis. SHELL43 elements, in contrast, allow for six degrees of freedom at each node. They also have plasticity, creep, stress stiffening, large deflection, and large strain capabilities making them the most realistic element for use in a 2D model [23].

The model also uses CONTAC52 elements at the bolt head to flange, nut to flange, inter-flange and rabbet interfaces. These gap elements are also given real constants to simulate stiffness and, at the nut/flange interface, interference is set to



account for initial bolt preload as was done earlier. Rabbets were given interference values as well, just as with the CONTAC12 elements of the original model. Both CONTAC12 and CONTAC52 elements are used to represent two surfaces in contact that may break contact and slide relative to one other. Both elements are also capable of supporting compression in a direction normal to the surfaces, and shear in the tangential direction. Unlike CONTAC52s, CONTAC12 elements only allow two degrees of freedom at each node. CONTAC52 elements allow for translation in the nodal x, y, and z directions. This is important due to the significant radial, axial, and tangential loads imparted by the nozzle and reacted at the nozzle support flange [23].

Once again PLANE25 elements are used throughout the rest of the model. These elements are typically used for two-dimensional modeling of axisymmetric structures such as in the case of the nozzle support. Four nodes with three degrees of freedom each define these elements. They allow for translation in the nodal x, y, and z direction. In the case of the nozzle support, these directions correspond to the radial, axial, and tangential directions, respectively [23]. With this definition we could reconstruct the joint from Figure 17 by replacing the BEAM3 elements with SHELL43 and CONTAC12 with CONTAC52 elements.

Material properties were also given to the gap elements to allow for friction between the members as was done in the previous model. Separate coefficients were used between flanges, at rabbets, and at the bolt head and nut to account for differences in clamp and assembly lubricant. In this model both the long and short bolts were accounted for as loads were split between the bolts directly connecting the flanges and those clamping the protective bolt shield.

The above-described modeling methodology for bolted joints was carried out at each bolted joint in the model. The remainder of the model, including applied loads, boundary conditions, and material properties, was the same as in the previous model. A view of the forward flange showing improved bolted joint modeling is shown in Figure 37. Note that the long and short bolts are shown on top of one another, as evident by conflicting meshes.

#### 4.2 PREDICTED FLANGE SEPARATION

Applying the same mechanical loads as in the previous case, flange separation was predicted. Temperatures were only accounted for in this model to determine changes in modulus, Poisson's ratio, conductivity, and specific heat. For the purposes of this investigation separation was considered between all flanges and at each rabbet location. Rabbets modeled with gap elements were given interferences and/or gaps based on current production geometry as shown in Figure 38.

When examining the gap between the combustor case and nozzle support, the model was divided according to the diagram in Figure 39 and nodes were selected along the interface. The white boxes along the boundary indicate node numbering. The model was then run and analyzed for the same time points as in the previous analysis. Again, this was a mechanical-only run that only included thermal effects as they related to certain material properties. The coefficients of thermal expansion were given zero values throughout the model. When relative axial displacements are plotted between the combustor case nodes and those along the support nozzle we find that a gap does exist throughout the mission at the outer diameter. The chart in Figure 40 suggests that clamp

is lost at the outer diameter but not at the bolt hole centerline. This falls in line with the predicted separation margin calculations conducted during initial joint design.

The chart also suggests flange leakage consistent with field findings where a gap is apparent at the outer diameter of the flange. It is important to reiterate that the numbered lines above correspond to the nodes shown in Figure 40. When compared with Figure 5, the gap predicted by the improved model implies accurate modeling. Taken together, the initial joint sizing and current modeling both reflect realistic behavior as witnessed on fielded hardware. To fully understand the impacts leakage might play, the rabbets of the joint were also examined during the mission. Figure 41 through 44 show rabbet locations and nodal selections along with predicted separation given an initial interference for both rabbet locations. Since the graphs from Chapter 3 indicate that these two rabbet interfaces are not open for significant amounts of time during the engine cycle, leakage through these interfaces is not considered. Also, other flange interfaces, between the seal and combustor case and between the bolt shield and nozzle support, are not taken into account since separation at these locations would not directly or significantly alter thermal gradients in the nozzle support flange.

#### 4.3 REVISED HEAT TRANSFER ANALYSIS

The heat transfer and flow networks were updated to include free vertical convection at the nozzle support-to-diffuser interface in accordance with the findings above. In this way, the joint is allowed to open up and more of the joint is exposed to the hot flowpath gases. This creates more gentle gradients in the flange at the outer diameter and a quicker response at the bolt hole centerline. Initial findings indicated that

temperatures in the joint were more even and the thermal gradient from the outside diameter to the bolt hole was reduced by approximately 118°F.

This difference was due to the changes in modeling technique. For stationary joints with high preload such as this, it is typical to assume little to no flange leakage. Contact resistance is often used to account for part-to-part contact. Heat transfer analysis generally recognizes that resistance between two parts is a function of how well those parts are held in contact. Several factors can alter that contact. Primarily, contact area, interface pressure, surface finish, and fluid present between the parts are considered. Often, for a bolted stationary flange contact pressure is assumed to be greater than 100 psi. For the bolted joint of concern however, significant preload was originally assumed to prevent any appreciable flange leakage. This, combined with a high bolt density, leads to the use of a convective heat transfer coefficient of 1,000 Btu / hr ft<sup>2</sup> °R. Had any leakage been present in the original assumptions, the heat transfer coefficient may have been much lower, 200-300 Btu / hr ft<sup>2</sup> °R. Figures 45 and 46 show the original and revised heat transfer models, respectively. In addition to including flange leakage, with a heat transfer coefficient of 200 at the bolt hole, the mesh was refined and more detail added. In fact, the heat transfer model needed to be modified to include the bolt. It is important to note that leakage assumptions were only modified at the joint of concern. No work was done to attempt to quantify leakage at any other joint.

Recent experience has shown the value of taking into account flange leakage in the thermal model. The importance of flange leakage in understanding engine performance and flange thermal responses has amplified the need to consider it during engine design. Field experience showing the impact of leakage on hardware has also

been critical. In fact, heat transfer engineers often use Fuller's Earth tests to better understand how bolted joints behave. Heat transfer engineers understand that leakage can play a big role in engine performance and flange LCF life and their analysis is scrutinized accordingly. Tradeoffs must be made and sound engineering judgment exercised when considering leakage. Often, increased leakage will yield higher flange LCF life and lower performance. Careful review and consideration is necessary to account for impacts to each.

The current 2D axisymmetric bolted joint modeling methodology employed by heat transfer engineers has greatly improved over the original analysis. The heat transfer analysis accounts for hole geometry and reduced conductivity and density accordingly. The actual bolt and nut are also included in the model so a complete stress analysis can be preformed. Previously only the hole was modeled and beam elements were used to apply the clamp. As the thermal model evolved, heat transfer engineers began viewing the bolt as a bar through which they could apply conduction. Now, the bolt and nut are modeled and meshed in the same manner as the structural hardware. Like the stress model, the heat transfer model is meshed with separate areas accounting for the flanges, the bolt holes, and the bolt and nut. In this way the bolt and nut materials can be identified and thermal properties can be assigned. As was done with orthotropic areas in the stress model, adjustments are necessary to account for the 3D features of the bolt and nut in the 2D representation. The bolt hole itself also requires adjustment. Pressures and thermal properties must be altered appropriately.

One adjustment necessary at the bolt holes is for conductivity. Material conductivity is modified to account for the number of bolt holes and their diameter. The equations for radial and axial conductivity multipliers are given below.

$$K_{mult, radial} = \frac{2\pi \left( \frac{r_1 + r_2}{2} \right) - ND}{2\pi \left( \frac{r_1 + r_2}{2} \right)} \quad (25a)$$

$$K_{mult, axial} = \rho_{mult} = \frac{\left( r_1^2 - r_2^2 \right) - \left( \frac{ND^2}{4} \right)}{\left( r_1^2 - r_2^2 \right)} \quad (25b)$$

N = number of holes

D = hole diameter

$r_1$  = radius to bolt hole inner diameter

$r_2$  = radius to bolt hole outer diameter

These reduction factors are critical in the proper representation of the bolt hole geometry. The above equation for radial conductive reduction is essentially a ratio of circumferences at the centerline with and without bolt holes. Likewise the axial multiplier contains elements of a simple area ratio again, with and without bolt hole. Reduction factors are also necessary for the bolt head, shank and nut. Without reduction factors the bolt and nut would appear in the model as solid rings. Therefore, the following factors are applied. Here again we see elements of area and circumferences.

$$K_{mult, radial} = \frac{ND}{2\pi \left( \frac{r_1 + r_2}{2} \right)} \quad (26a)$$

$$K_{mult, axial} = \rho_{mult} = \frac{\left( \frac{ND^2}{4} \right)}{\left( r_1^2 - r_2^2 \right)} \quad (26b)$$

Convection coefficients are then applied to the flanges, bolt, and nut. Area multipliers are used to account for the 2D representation of full 360° hardware. As a general rule, the area multiplier is a ratio of the actual physical area of the feature to its analytical representation as identified in Equation 27. Equations 28 through 30 then give the areas for actual and model geometry. These equations are used with Equation 27 to determine the area multiplier. It is important to note here that multipliers are necessary for the bolt head, shank and nut as well as the flange faces.

$$\text{Area multiplier} = \frac{\text{Physical Area}}{\text{Area Calculated by } P_{\text{thermal}}} \quad (27)$$

$$A_{\text{head}} = \pi N \left( Dt + \frac{D^2}{4} \right) \quad (28a)$$

$$A_{P_{\text{thermal}}} = \pi \left[ (r_1^2 - r_2^2) + 2t(r_1 + r_2) \right] \quad (28b)$$

D = Average diameter of bolt shank and nut

t = width of exposed shank and nut

N = number of bolts

$$A_{\text{face}} = \pi \left[ (r_1^2 - r_2^2) - \frac{ND^2}{4} \right] \quad (29)$$

$$A_{P_{\text{thermal}}} = \pi (r_1^2 - r_2^2)$$

Area multipliers are also necessary for the contacts between the bolt and flange, nut and flange, between flanges, and between the flanges and nut and the bolt shank. Appropriate equations are listed below.

$$A_{contact} = \pi N(r_1^2 - r_2^2) \quad (30a)$$

$$A_{Pthermal} = \pi(r_o^2 - r_i^2) \quad (30b)$$

$$A_{mult} = \frac{A_{contact}}{A_{Pthermal}} = \frac{N(r_1^2 - r_2^2)}{(r_o^2 - r_i^2)} \quad (30c)$$

$r_o$  = outer radius of contact face

$r_i$  = inner radius of contact face

$$A_{contact} = \pi \left[ (r_o^2 - r_i^2) - \frac{ND^2}{4} \right] \quad (31a)$$

$$A_{Pthermal} = \pi(r_o^2 - r_i^2) \quad (31b)$$

$$A_{mult} = \frac{A_{contact}}{A_{Pthermal}} = 1 - \left[ \frac{\frac{ND^2}{4}}{(r_o^2 - r_i^2)} \right] \quad (31c)$$

$$A_{contact} = \pi NDt \quad (32a)$$

$$A_{Pthermal} = 2\pi(r_o + r_i)t \quad (32b)$$

$$A_{mult} = \frac{A_{contact}}{A_{Pthermal}} = \frac{ND}{2(r_o + r_i)} \quad (32c)$$

These geometric multipliers are then applied to a Patran™ model. Patran™ is a pre and post-processor available from MSC Software that allows advanced modeling and the creation of finite element models. Heat transfer engineers use Patran™ to import UG models, mesh the geometry, and apply boundary conditions. They then use P/Thermal (Patran™ Thermal), a thermal management solver developed for use in aerospace modeling. After the run in P/Thermal is complete, the results are brought back into Patran™ for review and post-processing [27].



P/Thermal is able to read in the finite element information from the Patran™ database and construct mathematical resistor/capacitor sets that define the thermal model. Unlike stress models, P/Thermal does not use approximating equations. Instead, the actual heat transfer defined is analyzed. P/Thermal is able to account for conduction, convection, radiation and advection using simple electrical analogies. For example, for conduction between two features the following equation is applied.

$$Q_{1 \rightarrow 2} = \frac{T_1 - T_2}{R} \quad (33)$$

In the above relation, R is the resistance between the features. A typical 1D Cartesian resistance would be calculated as follows.

$$R = \frac{Length}{k * Area} \quad (34)$$

Similarly conductance, G, is calculated as 1/R. Similar equations exist for convection, advection, and radiation. P/Thermal can analyze steady-state as well as transient solutions like the one identified for the hardware of concern. Although Patran™ and P/Thermal were used for the original analysis, as indicated earlier, treatment of the bolt is greatly improved. Modeling the bolt as a 2D representation of 3D hardware, complete with conductive and convective heat transfer, allows for a more accurate and complete model. Assuming gaps and leakages that correspond to fielded hardware, engine tests, and mechanical loading, realism has been added to the analysis. Heat transfer engineers currently enter into new designs paying greater attention to leakage assumptions and, where possible, 3D sub-models are used to fully understand hardware behavior. It is important to note that the equations listed above for bolt area multipliers,

conduction, convection, etc. were not in the original model developed decades ago. This alone is a significant improvement in the bolted joint analysis.

#### 4.4 REVISED STRUCTURAL ANALYSIS AND LCF CALCULATIONS

Following the modification of the heat transfer model, the new thermal results were incorporated into the stress model. The thermal analysis revealed a gradient more than 100°F lower than the original model prediction at the takeoff time point. The baseline and improved model flange temperature gradients throughout the mission are visible in Figure 47. At steady state conditions, the differences in gradient are not severe. At takeoff and during other transients however, significant differences in gradient magnitude are evident. Performing the ANSYS® analysis for the same time points initially chosen, stresses were determined at the interface. Overall, hoop stress decreased by more than 25ksi at takeoff. Hoop stress is the most significant driver of flange LCF life at the bolt hole and is greatly impacted by flange gradients as identified in example plotted in Figure 48. Using the same methodology to calculate life at the bolt hole as in Section 3.6, a low cycle fatigue analysis resulted in life exceeding 2X at the most limiting location at the bolt hole. Again, for the basis of this paper, X is the original life in cycles of the flange following the original modeling methodology. Clearly leakage assumptions play a part in flange LCF life calculations at bolted joints. Although this is an improvement, it is not enough to explain high, fielded life exceeding 3X. Over the existing model, LCF life at the nozzle support flange increased by a factor of two. In an effort to further scrutinize the model and modeling assumptions equations, inputs and constraints were reevaluated.

#### 4.5 FIGURES

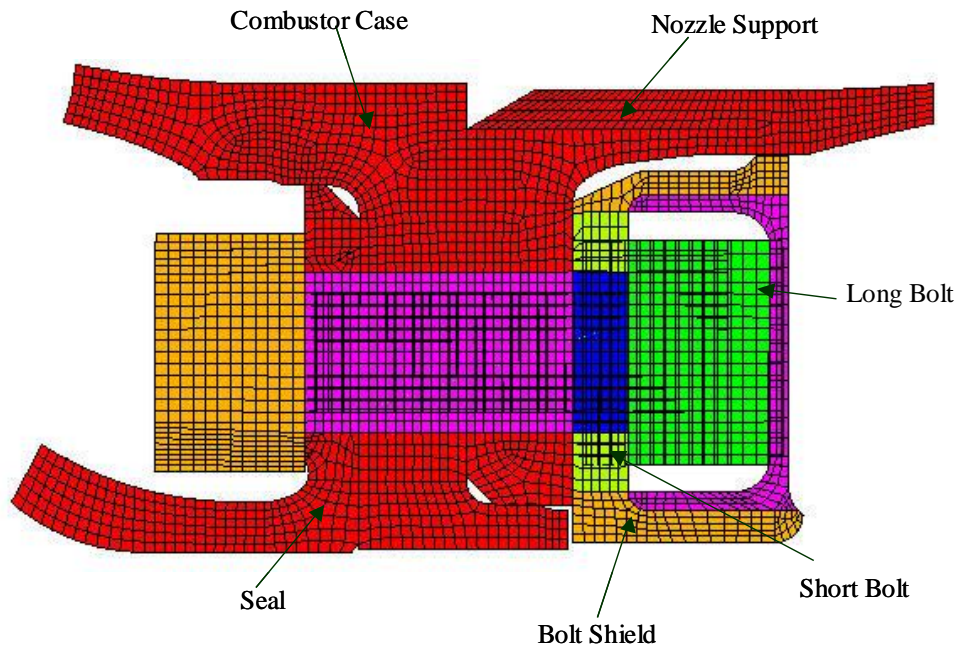


Figure 34: Improved Bolted Joint Modeling

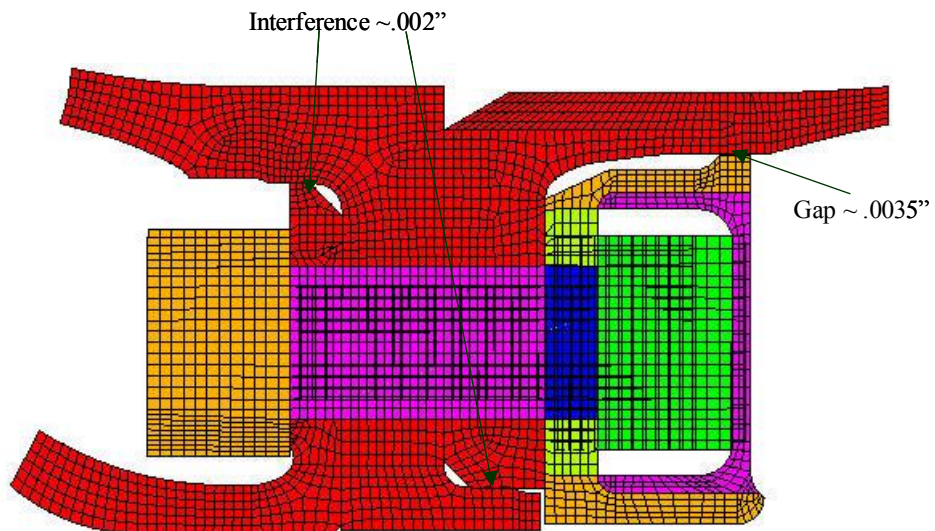


Figure 35: Rabbet Interference/Gap Definition and Location

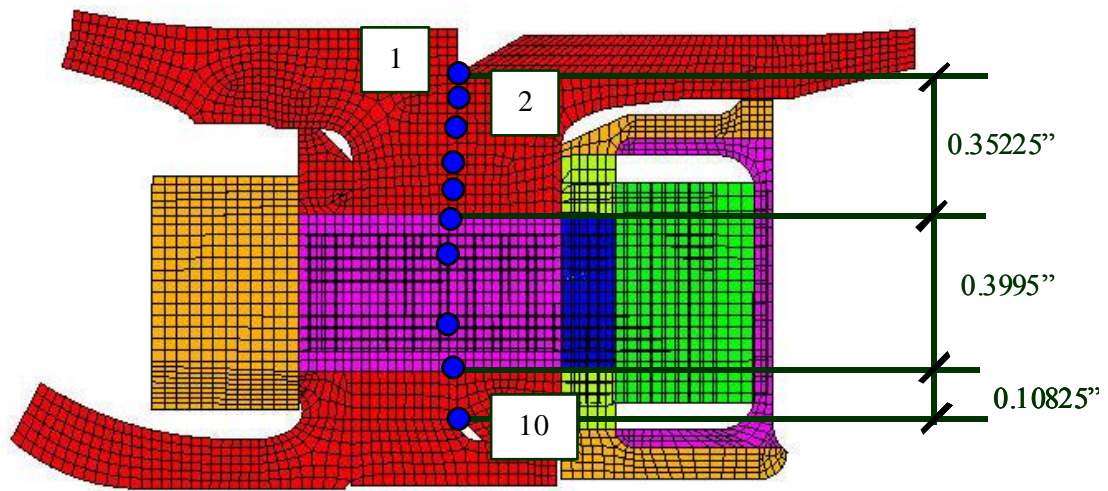


Figure 36: Combustor Case/Nozzle Support Interface Selected Nodes

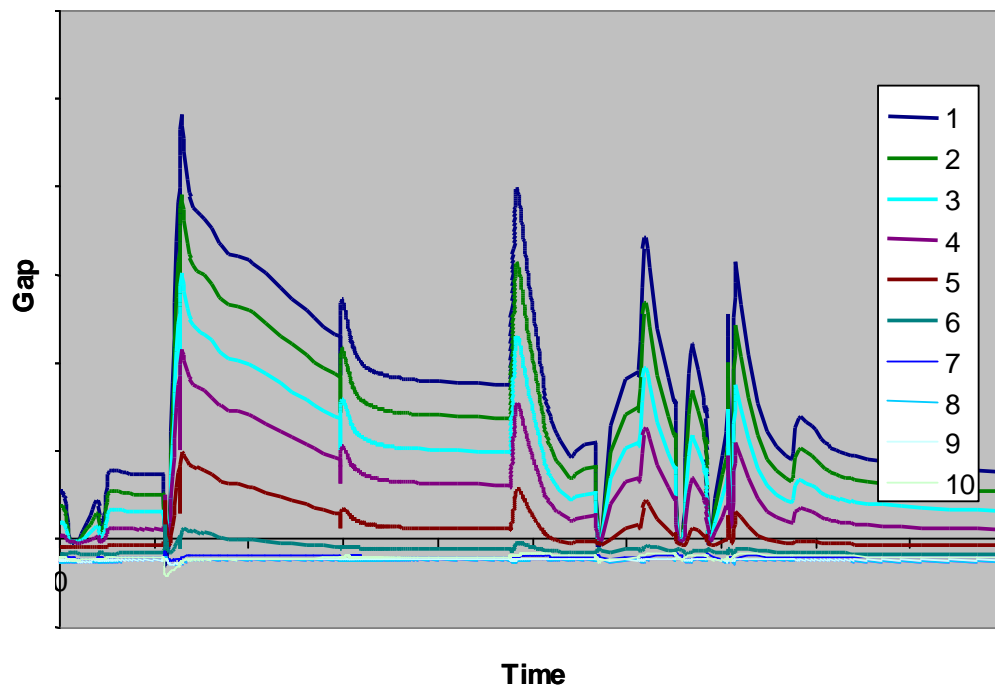


Figure 37: Combustor Case/Nozzle Support Gap vs. Mission Time

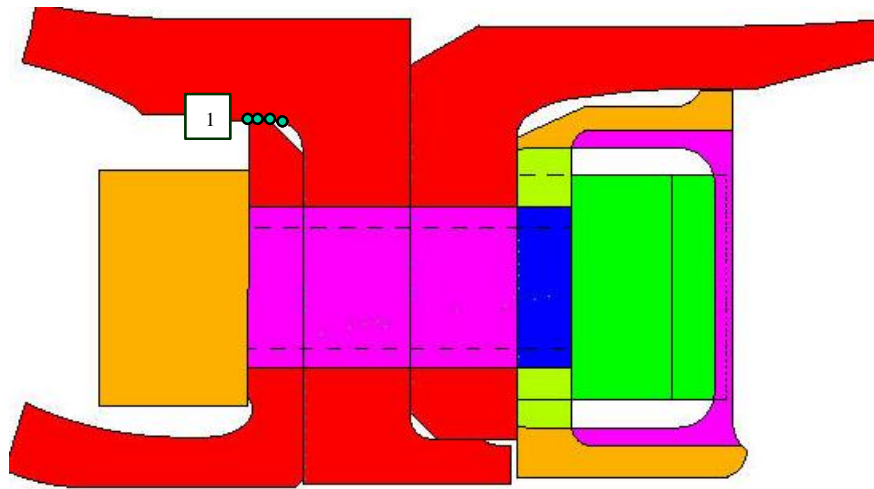


Figure 38: Seal/Combustor Case Rabbit Selected Nodes

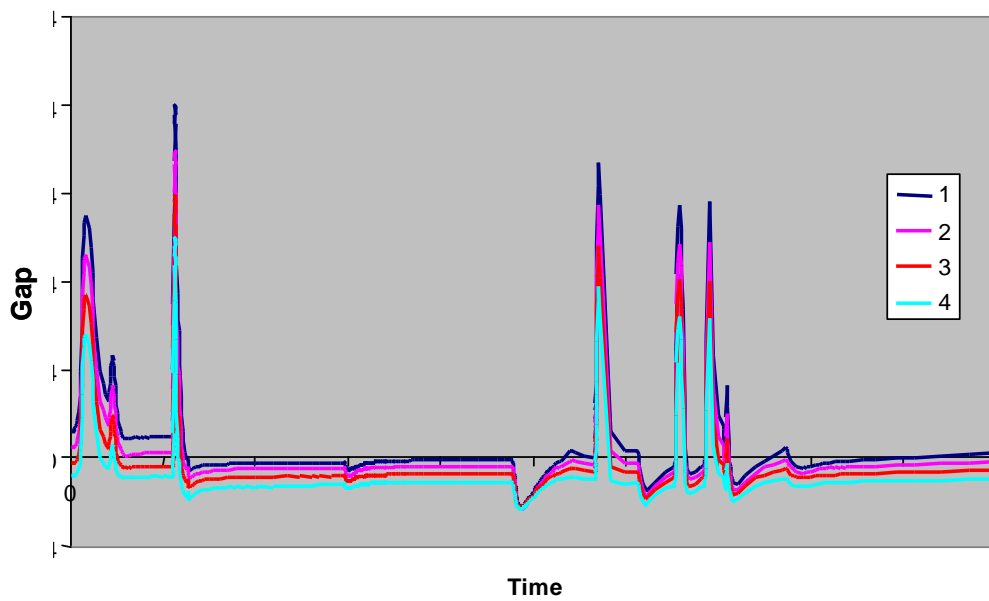


Figure 39: Seal/Combustor Case Gap vs. Mission Time

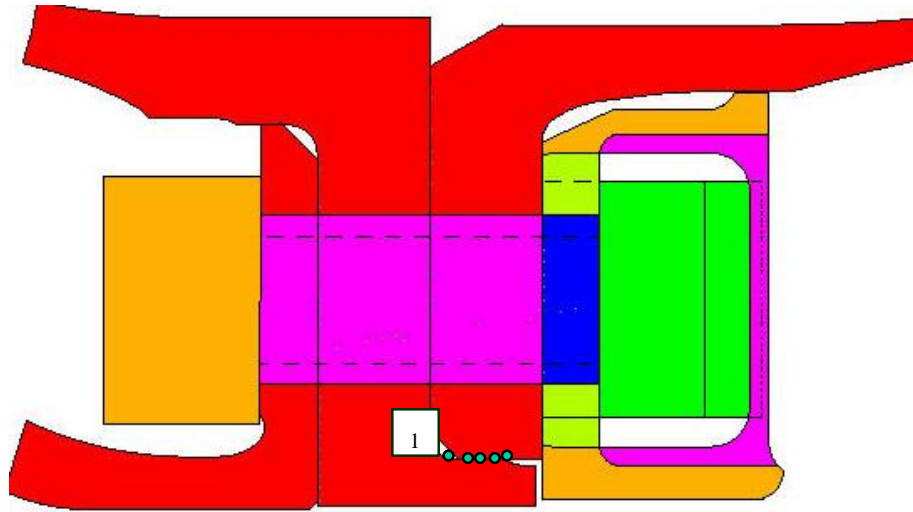


Figure 40: Combustor Case/Nozzle Support Rabbet Selected Nodes

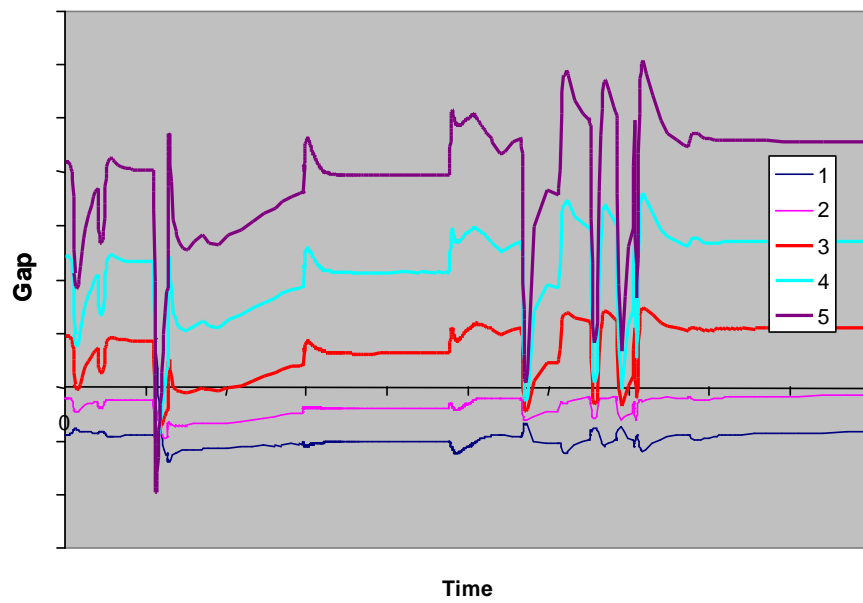


Figure 41: Combustor Case/Nozzle Support Gap vs. Mission Time

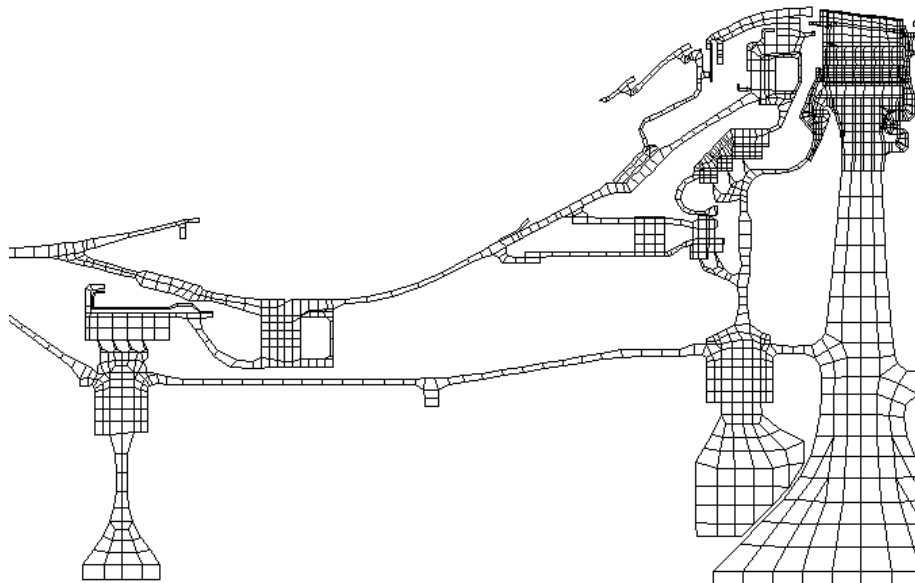


Figure 42: Original Heat Transfer Model

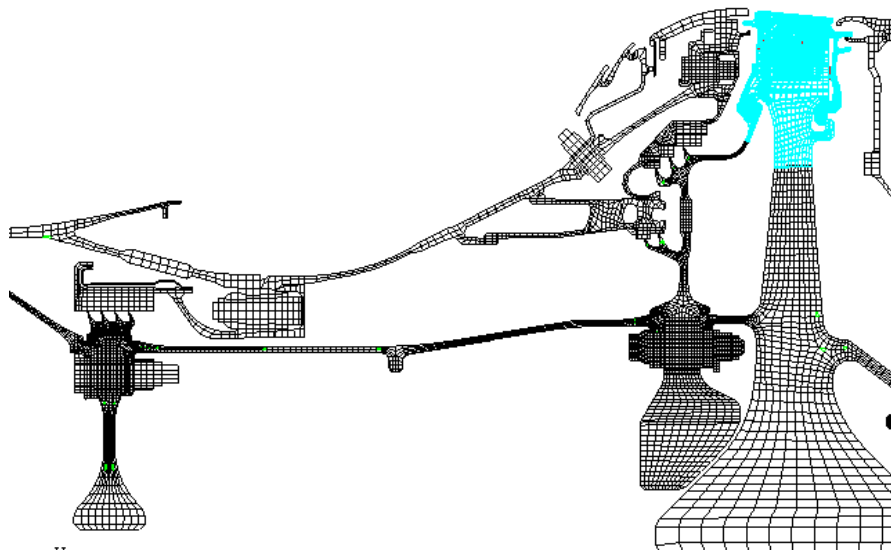


Figure 43: Updated Heat Transfer Model

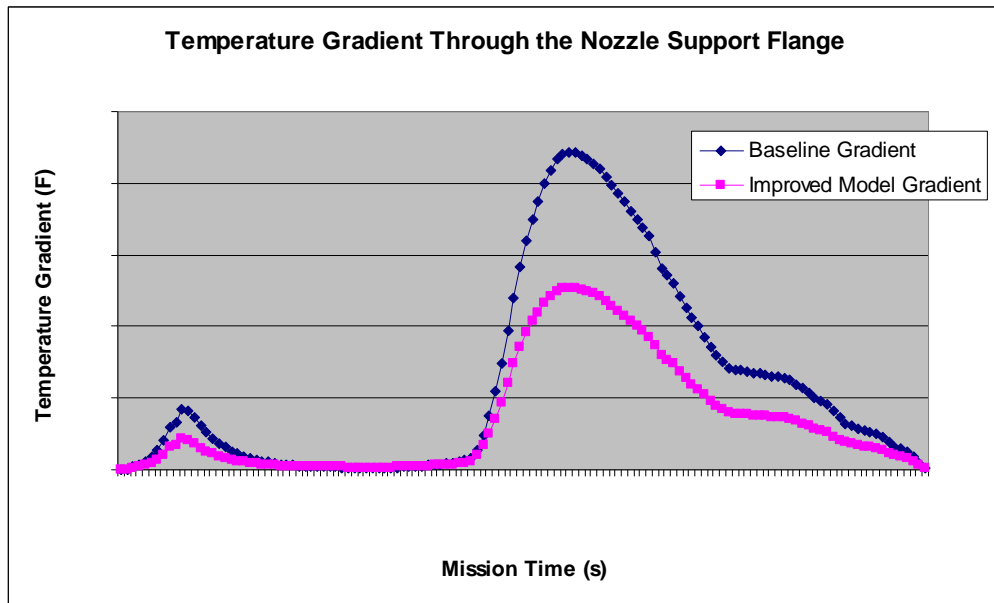


Figure 44: Flange Temperature Gradients vs. Time Baseline and Improved Model

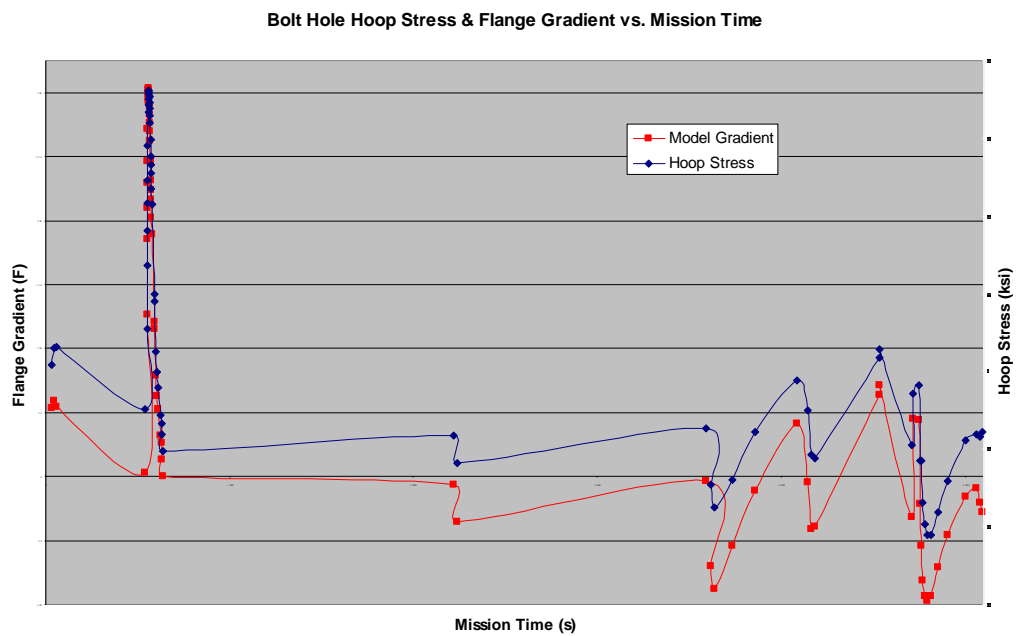


Figure 45: Flange Temperature Gradient and Hoop Stress vs. Time



## **CHAPTER 5**

### **CONCLUSIONS**

#### **5.1 LCF LIFE COMPARISON**

Although the improved modeling predicts higher LCF life than the original analysis, it does not fully explain why the flange in the field seems capable of 3-4X cycles. Differences over predicted life values cannot be wholly accounted for by flange leakage. It is however, a significant shift toward more accurate modeling of the joint in question. A closer inspection of inherent assumptions shows that material property curves can also play a significant part in LCF life determination.

Examining our assumptions more closely we find that our life calculations assume minimum material properties as described earlier. This conservative assumption is made to protect against hidden material defects inherent in manufacturing processes that are not easily detectable during non-destructive evaluation (NDE). Although these rolled ring forgings are put through extensive verification testing, material defects are nearly impossible to guard against completely. For a comparison, lives at the nozzle support forward flange were evaluated using average material properties. This analysis was conducted by simply comparing alternating pseudostress to average, instead of minimum, material curves. Calculations revealed that under the original analysis methodology, assuming the flanges do not separate, life at the nozzle support flange exceeds 2X. With the new methodology, allowing leakage due to flange separation, we find that life and nozzle support bolt hole is 3X, much closer to witnessed hardware behavior.

Undoubtedly the conservatism necessary in accounting for material defects can lead to low predicted LCF life. Average material properties however, may not be assumed for the hardware in this joint. Although the fielded life may be explainable given the LCF benefit due to material property conditions, federal mandates require LCF determination to minimum properties. Even if on a statistical basis the probability of a fielded part containing minimum properties is remote, the inherent uncertainty and possible consequences of this assumption command conservatism. In order to show sufficient life, as verified by the Federal Aviation Administration (FAA), we must life the part assuming minimum properties.

One area of particular concern is the assumed  $h$  multiplier used in the area of the forward flange. As noted earlier,  $h$ 's are higher than typically used due to validation with recent engine tests. Typical values of  $h$  include a multiplier of  $Y$ . Due to testing in the 1990s the  $h$  multiplier at the nozzle support forward flange was increased to  $2Y$ . It is believed however, that the thermocouples used during the testing read air temperatures instead of metal temperatures. Calculated  $h$  multipliers were therefore increased for data matching. Further examination is needed into this issue and more engine tests and thermal surveys will be necessary. An investigative look at the impact  $h$  multipliers can have is depicted in the chart in Figure 49. Although the temperature scale is removed, the temperature shift represented in the chart is not insignificant. Test data collected from thermocouple readings in the late 1990's appears in blue. The red and green lines show the gradient assuming  $h$  multipliers of  $2Y$  and  $Y$ , respectively. It is evident that the  $h$  multiplier value used in the model is key. It is important to note that  $h$  multiplier data in the chart stems from a special heat transfer model created to simulate test conditions.

This model was built allowing the user to easily change  $h$  multiplier values to arrive at flange temperature values. Comparing the reduced gradient possible with a lower assumed  $h$  multiplier value with LCF life calculations we find that life is improved by roughly the same amount as when leakage is included. Like the flange leakage assumption, it appears that the  $h$  multiplier used in the model may not fully account for higher field life. Instead, a combination of leakage and appropriate multiplier may be necessary to completely understand actual hardware performance.

## 5.2 ONGOING EFFORTS

Quantifying leakage and obtaining accurate temperature readings during engine testing are constant concerns for heat transfer, mechanical, and test engineers. With the certification of each new engine and during upgrade testing for existing product lines, engineers responsible for hardware around the joint of concern will focus intently on obtaining useful data. In fact, recent certification and block tests were conducted to simulate engine operating conditions for a scaled down variant of this commercial powerplant. Data have yet to be analyzed but this, and future tests will further the understanding of joint leakage, heat transfer assumptions, and predicted LCF life.

For future tests, engineers will continue to take great care to ensure thermocouples are placed appropriately. Thermocouples will also be positioned to measure metal and air temperatures. This will give engineers a good idea as to what heat transfer coefficients were applied in the past and which ones should be applied in the future. Although it remains unclear as to what factors are at play in the lower than witnessed predicted flange life, it is evident that flange leakage plays an important role.

Continued inclusion of leakage in this and future analysis will ensure that, as technology progresses, the analysis will continue to evolve as engineers strive for realism.

### 5.3 FIGURES

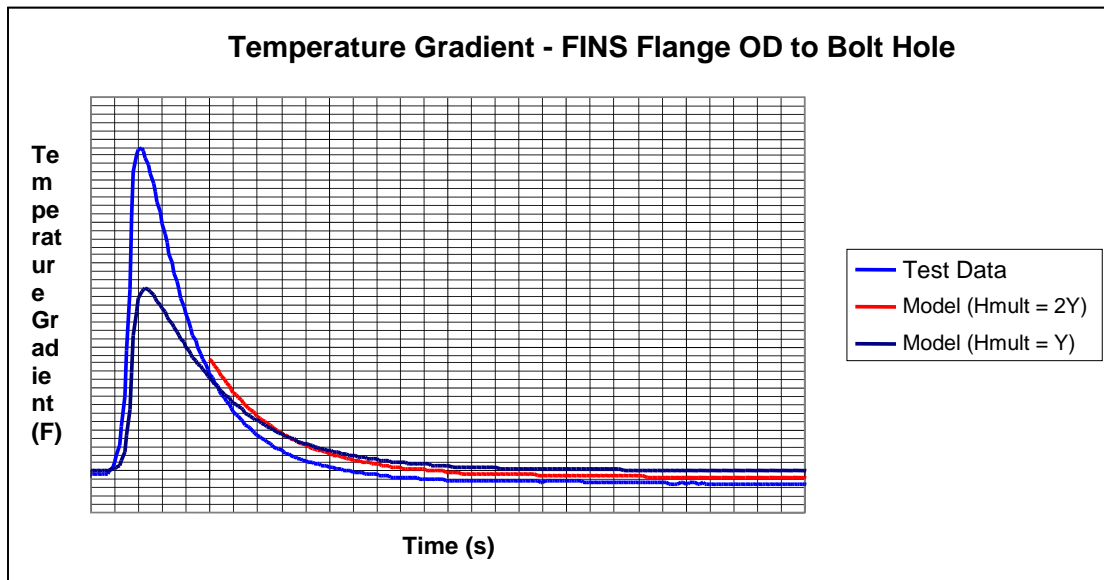


Figure 46: H Multiplier Impact

## REFERENCES

- [1] Maymon, Giora, *Structural Dynamics and Probabilistic Analysis for Engineers*, Elsevier, Burlington, MA, 2008.
- [2] Blake, Alexander, *Design of Mechanical Joints*, Marcel Dekker Inc., New York, 1985.
- [3] Madenci, E., Guven I., *The Finite Element Method and Applications in Engineering Using ANSYS*, Springer, 2005.
- [4] Bickford, J., *Introduction to the Design and Behavior of Bolted Joints, Fourth Edition*, CRC Press, Boca Raton, FL, 2008.
- [5] Abernethy, R., *The New Weibull Handbook, Fifth Edition*, Robert B. Abernethy, North Palm Beach, FL, 2004.
- [6] Hagiwara, M., Yoshimoto, I., *Fatigue Design of Bolted Joint Taking Into Account Reliability Concepts*, Experimental Mechanics, 1986, Vol. 27, p. 398-403.
- [7] Abid, M., Hussain, S., *Relaxation Behaviour of Gasketed Joints During Assembly Using Element Analysis*, Sadhana, 2010.
- [8] Kim, J., Yoon, J., Kang, B., *Finite Element Analysis and Modeling of Structures with Bolted Joints*, Applied Mathematical Modeling, 2006, vol. 31, p. 895-911.
- [9] Spence, J., Macfarlane, D., Tooth, A., *Metal-to-Metal Full-Face Taper-Hub Flanges: Finite Element Model Evaluation and Preliminary Plastic Analysis Results*, Proceedings Institution of Mechanical Engineers, 1998, Vol. 212, p. 57-69.
- [10] Nash, D., Spence, J., Tooth, A., Abid, M., Power, D., *A Parametric Study of Metal-to-Metal Full-Face Taper-Hub Flanges*, International Journal of Pressure Vessels and Piping, 2000, vol. 77, p. 791-797.
- [11] Moaveni, S., *Finite Element Analysis: Theory and Application with ANSYS*, Prentice Hall, Upper Saddle River, NJ, 2007.
- [12] Abid, M., Nash, D., *Comparative Study of the Behavior of Conventional Gasketed and Compact Non-gasketed Flanged Pipe Joint Under Bolt Up and Operating Conditions*, International Journal of Pressure Vessels and Piping, 2003, vol. 80, p. 831-841.

- [13] Bouzid, A., Chaaban, C., *An Accurate Method for Evaluating Relaxation in Bolted Flanged Connections*, ASME Journal, Pressure Vessel Technology 1997, 199, 10-17.
- [14] Bouzid, A., Beghou, H., *The Design of Flanges Based on Flexibility and Tightness*, Proceedings of the 2003 ASME-PVP Conference, PVP2003-1883, Cleveland, OH, Vol. 457, p. 31-38.
- [15] Bouzid, A., Nechache, A., *Thermally Induced Deflections in Bolted Flanged Connections*, ASME Journal Pressure Vessel Technology, 2005, 127, 394-401.
- [16] Bouzid, A., Nechache, A., *Creep Analysis of Bolted Flange Joints*, International Journal of Pressure Vessels and Piping, 2006, vol. 85, p. 185-194.
- [17] Fukuoka, T., *Unique Finite Element Analysis of the Thermal and Mechanical Behaviors of a Bolted Joint*, ASME Journal Pressure Vessel Technology, 2005, 127, 402-407.
- [18] Bouzid, A., Nechache, A., *An Analytical Solution for Evaluating Gasket Stress Change in Bolted Flange Connections Subjected to High Temperature Loading*, ASME Journal Pressure Vessel Technology, 2005, 127, 414-422.
- [19] Hyde, T., Lewis L., Fessler, H., *Bolting and Loss of Contact Between Cylindrical Flat-Flanged Joints Without Gaskets*, Journal of Strain Analysis, 1988, Vol. 23, p. 1-8.
- [20] Czachor, Robert P., *Unique Challenges for Bolted Joint Design in High-Bypass Turbofan Engines*, 2003 ASME Turbo Expo: Power for Land, Sea, and Air, Atlanta, June 2003.
- [21] Bickford, J., Nassar, S., *Handbook of Bolts and Bolted Joints*, Marcel Dekker, Inc. New York, NY, 1998.
- [22] Kulak, G., Fisher, J., Struik, J., *Guide to the Design Criteria for Bolted and Riveted Joints, Second Edition*, John Wiley & Sons, Inc., New York, NY, 1987.
- [23] "ANSYS® v. 11.0 Theory Reference," ANSYS® Inc., 2007.
- [24] Pilkey, Walter D., *Peterson's Stress Concentration Factors Second Edition*, John Wiley & Sons, Inc., New York, 1997.
- [25] Gyekenyesi, J.Z., Murthy, P.L.N., Mital, S.K., *NASALIFE—Component Fatigue and Creep Life Prediction Program*. NASA/TM-2005-213886. National Aeronautics and Space Administration: Washington, DC; 2005.

- [26] American Society for Testing and Materials, “E 1049–85 (Reapproved 2005) Standard Practice for Cycle Counting in Fatigue Analysis.” ASTM International, West Conchohocken, PA, 2010.
- [27] “Patran™ The Industry’s Leading Finite Element Modeling Environment,” MCS Software Corporation, 2008.
- [28] Mattingly, J., Heiser, W., Pratt, D., *Aircraft Engine Design*, American Institute of Aeronautics and Astronautics, Inc. Reston, VA, 2002.
- [29] Sawa, T., Takagi, Y., Torii, H., Yamada, K., *The Sealing Performance of a Large Diameter Bolted Joint Under Elevated Temperature*, ASME 2007 Pressure Vessels and Piping Conference, San Antonio, 2007.



## **AUTHOR'S BIOGRAPHY**

Christopher Carter was born in Columbus, Ohio, on August 24, 1977. He graduated from the United States Military Academy at West Point with a degree in Mechanical Engineering in 2000. He served five years in the United States Army as a Military Intelligence Officer with the 3D Infantry Division in Fort Stewart, GA. During his service he saw combat in Iraq as Intelligence Officer for the 1-64 Armor Battalion. As he left service he attended the University of Indiana's Kelley School of Business and received an MBA in 2004. Chris currently works for General Electric – Aviation in Cincinnati, Ohio as a design engineer.